High dimensional tori and chaotic and intermittent transients in magnetohydrodynamic Couette flows

F. Garcia,[1] J. Ogbonna,[2] A. Giesecke,[2] and F. Stefani[2]
[1)] *Department of Fluid Mechanics, Universitat Politècnica de Catalunya, Avda. Eduard Maristany 16, 08019 Barcelona, Spain*
[2)] *Department of Magnetohydrodynamics, Helmholtz-Zentrum Dresden-Rossendorf, Bautzner Landstraße 400, D-01328 Dresden, Germany*

(Dated: 19 January 2023)

The magnetised spherical Couette (MSC) problem, a three dimensional magnetohydrodynamic paradigmatic model in geo- and astrophysics, is considered to investigate bifurcations to high-dimensional invariant tori and chaotic flows in large scale dissipative dynamical systems with symmetry. The main goal of the present study is to elucidate the origin of chaotic transients and intermittent behaviour from two different sequences of Hopf bifurcations involving invariant tori with four fundamental frequencies, which may be resonant. Numerical evidence of the existence of a crisis event destroying chaotic attractors and giving rise to the chaotic transients is provided. It is also shown that unstable invariant tori take part in the time evolution of these chaotic transients. For one sequence of bifurcations, the study demonstrates that chaotic transients display on-off intermittent behaviour. A possible explanatory mechanism is discussed.

I. INTRODUCTION

Numerical simulations are nowadays a fundamental tool to advance in the field of geophysical and astrophysical fluid dynamics. Canonical models describing the motion of electrically-conducting fluids are derived from the well-known Navier-Stokes and induction equations (Moffatt and Dormy (2019)). These are time-dependent and nonlinear partial differential equations whose analytic solution is unknown and therefore numerical algorithms are developed for the approximation of their solution with computer simulations. The analysis of simulation data when contrasted with observations helps to develop more accurate theoretical dynamo models of geo- and astrophysical phenomena (Roberts and Glatzmaier (2000)). In addition, simulations also provide valuable information for the design and guiding of experiments in the field (Gailitis *et al.* (2002)).

One of the classical examples of a geophysical and astrophysical problem is the magnetised spherical Couette (MSC) problem in which a conducting fluid fills the gap between two differentially rotating spheres in the presence of a magnetic field applied parallel to the axis of rotation. This problem has been widely studied both numerically (Hollerbach (2009); Travnikov, Eckert, and Odenbach (2011); Gissinger, Ji, and Goodman (2011); Garcia *et al.* (2020a)) as well as experimentally (Sisan *et al.* (2004); Kasprzyk *et al.* (2017); Kaplan, Nataf, and Schaeffer (2018); Barik *et al.* (2018); Ogbonna *et al.* (2020, 2022)) due to its relevance to understanding the origin and evolution of planetary and stellar flows.

In the mathematical formulation of the MSC problem, three dimensionless parameters describe the input physics. They are the aspect ratio of the spherical shell $\chi = r_i/r_o$ (r_i and r_o are the inner and outer radii, respectively), the Reynolds number Re measuring the differential rotation, and the Hartmann number Ha measuring the strength of the applied magnetic field. As these parameters are varied, a rich variety of dynamical regimes have been discovered, described, and analysed during the last decades thanks to the use of numerical simulations (e. g. Hollerbach and Skinner (2001); Hollerbach (2009); Travnikov, Eckert, and Odenbach (2011); Gissinger, Ji, and Goodman (2011); Kaplan (2014); Kaplan, Nataf, and Schaeffer (2018); Garcia *et al.* (2020a)). For instance, for a given relatively thin shell geometry ($\chi \geq 0.5$) and for all magnetic field strengths (Ha), a time independent and axisymmetric (i. e. invariant by any azimuthal rotation) base state is found for sufficiently small differential rotation (Re). With increasing Re, this base state becomes unstable to a non-axisymmetric instability, with some azimuthal symmetry $m = m_1$ (m is the azimuthal wave number), whose spatial nature strongly depends on Ha. For low Ha, the instability is basically hydrodynamic and situated at the radial jet flowing outwards in the equatorial plane. At moderate Ha, the instability takes the form of a return flow concentrated in the middle of the shell, and for larger Ha, the flow streamlines are basically parallel to the axis of rotation, giving rise to the shear-layer instability.

These dynamical regimes are subjected to the symmetries of the MSC system, which is an $\mathbf{SO}(2)\times\mathbf{Z}_2$ equivariant system, meaning that it is invariant to azimuthal rotations and reflections with respect to the equatorial plane. Theoretical studies in the framework of dynamical systems with symmetry (Crawford and Knobloch (1991); Ecke, Zhong, and Knobloch (1992); Golubitsky and Stewart (2003)) have demonstrated that the Hopf-like instability of the axisymmetric base state gives rise to rotating waves (RW), a type of periodic flow with certain azimuthal symmetry $m = m_1$ for which the time evolution is described as a solid body rotation of a fixed flow pattern (Garcia and Stefani (2018)). A secondary Hopf bifurcation is responsible for the appearance of modulated rotating waves (MRW) which are quasiperiodic flows with two fundamental frequencies, i. e. invariant

two dimensional tori (Rand (1982); Golubitsky, LeBlanc, and Melbourne (2000); Casas and Jorba (2012); Garcia *et al.* (2019)). Successive Hopf bifurcations, for which a symmetry breaking occurs, give rise to high-dimensional invariant tori with three (Garcia *et al.* (2020a)) and even four fundamental frequencies (Garcia *et al.* (2020b)). The analysis of symmetry breaking bifurcations of MRW in symmetric systems is of fundamental importance since they enable the Newhouse-Ruelle-Takens theorem (Newhouse, Ruelle, and Takens (1978)) to be overcome in the route to chaotic flows.

This paper concentrates on the analysis of high-dimensional tori (with dimensions of 2,3 and 4) and the bifurcations to chaotic flows, which have been recently discovered by Garcia *et al.* (2020b), but also investigates the presence of transient phenomena associated with the disappearance of a chaotic attractor. An exploration of the parameter space leads us to the identification of resonant invariant four-dimensional tori and also to detect and investigate intermittent behaviour during chaotic transients. Invariant tori, and their bifurcations to chaotic flows, are widely studied in the case of low dimensional systems. For instance, the appearance and disappearance of four-dimensional tori and chaotic attractors have been studied in detail by Kuznetsov, Sataev, and Turukina (2011) for a system of three coupled van der Pol oscillators. Quasiperiodic invariant tori, including resonant motions and global bifurcation to chaotic flows, have also been comprehensively investigated by Fleurantin and James (2020) in the case of a three dimensional dissipative vector field. For high-dimensional systems arising from the discretisation of partial differential equations the computational methods of regular states require the implementation of parallel algorithms based on advanced numerical linear algebra methods (e. g. Dijkstra *et al.* (2014); Tuckerman (2020)). For this reason the exploration of both the parameter as well as the phase space in this type of problems is restricted by the computational resources and thus there exist few studies addressing global bifurcations of high-dimensional tori and chaotic flows. This is in particular the case for the MSC system considered in our study.

A crisis event (Grebogi, Ott, and Yorke (1982, 1983)) is one of the most common mechanisms by which a chaotic attractor loses stability in favour of a chaotic saddle. The latter comprises nonattracting invariant sets in the phase space which are responsible for chaotic transient phenomena. Transient chaos is however not only associated with chaotic saddles but may be also due to the existence of a blow-out bifurcation (Ott and Sommerer (1994)), and even other mechanisms (see Omel'chenko and Tél (2022) for a review). The global properties of chaotic attractors, the structure of their basin of attraction (Sommerer and Ott (1993)), and the bifurcations giving rise to them in nonlinear systems, are nowadays an active area of research. This is especially true in the case of low-dimensional systems such as the Duffing-Van der Pol oscillator and related problems (e. g. Yue, Xu, and Wang (2013); Feng (2017)), but also for problems in other disciplines such as economics (Lorenz and Nusse (2002)).

Chaotic motion can be intermittent, in the sense that the time evolution of the system alternates between two or more different states that occupy distinct regions in the phase space (see the review of Knobloch and Moehlis (1999)). Different types of intermittent dynamics, type-I, II, and III, were studied in Pomeau and Manneville (1980) in the context of the Lorenz problem with the aim of shedding light on the observed behaviour in fluid dynamics experiments. In their description, the different types of intermittence arise from the different ways in which a simple fixed point of the system loses stability as a control parameter is varied. Intermittent behaviour may also arise as a result of certain types of crisis for which a chaotic attractor suddenly changes its distribution in the phase space (Grebogi *et al.* (1987)). Unstable invariant objects, lying on an invariant manifold of the phase state, organise on-off intermittent behaviour defined in Platt, Spiegel, and Tresser (1993). In this latter study, the fact that the stability of these unstable orbits is controlled by dynamics outside from the manifold resulted in a key issue. The special type of on-off intermittency may appear as a result of a blow-out bifurcation (Ott and Sommerer (1994); Ott *et al.* (1995)) when the chaotic attractor losing stability does not have a riddled basin of attraction. The existence of intermittent behaviour has also been associated with an orbit riddling (He (2005)), after a tangency in the phase space is developed from high-dimensional tori, once the parameter is varied in a one dimensional nonlinear wave system.

In the fluid dynamics context, such as the plane Couette or pipe flows (Eckhardt *et al.* (2008); Budanur, Dogra, and Hof (2019); Letellier (2017)) the analysis of transient chaos and chaotic saddles has provided valuable insight in the understanding of the transition to turbulence, the formation of coherent structures, and the characterisation of intermittent behaviour. In the concrete case of shear flows, the concept of intermittency has been of importance to understand transition to turbulence (Avila and Hof (2013); Lemoult *et al.* (2016)). Depending on the aspect ratio of the container the transition to turbulence could have a spatio-temporal nature, or in contrast, could be mainly described as a purely temporal process (Philip and Manneville (2011)). The existence of these unstable states and their invariant manifolds (e. g. Gibson, Halcrow, and Cvitanović (2008); Kawahara, Uhlmann, and van Veen (2012)) is key for describing the laminar-turbulant boundary and coherent structures in shear flows. According to van Veen and Kawahara (2011), a homoclinic tangle between the stable and unstable manifolds is responsible for chaotic intermittent bursting. Later, Cherubini and De Palma (2013) conjectured that the existence of bursts can be also described by heteroclinic connections approaching an unstable periodic orbit. A systematic computation and description of heteroclinic connections, a structurally

stable solution departing from unstable equilibria or periodic orbits and tending to another unstable regular flow, has been performed in Halcrow *et al.* (2009).

The analysis of intermittent chaotic motion in three dimensional MHD systems in the framework of dynamical systems theory is also fundamental for understanding how cosmic magnetic fields are generated (Pratt, J., Busse, A., and Müller, W.-C. (2013)) but also to shed light into the formation of coherent structures in astrophysical plasmas (Matthaeus *et al.* (2015)). In the case of numerical simulations within a periodic box (e. g. Sweet *et al.* (2001); Alexakis and Ponty (2008)), dynamo action takes place as a result of a blow-out (non-hysteretic) bifurcation with associated on-off intermittency. This is also the case for the MSC dynamo problem (Raynaud and Dormy (2013)), in which the magnetic field is not externally applied as in our case. However, in the case of the α^2 dynamo model of Oliveira *et al.* (2021), intermittent behaviour was not found and the dynamo effect saturates thanks to a hysteretic blow-out bifurcation. Dynamo experiments in a turbulent background have also shown intermittent magnetic field measurements (Nornberg *et al.* (2006)).

This paper starts by describing the MSC system of equations and the numerical methods employed to solve them in Sec. II. The selected output data and the methods employed to analyse it are outlined in Sec. III. The paper then mainly addresses two important aspects described above. Firstly, we provide further evidence of the bifurcation scenario first described in Garcia *et al.* (2020b) by presenting a new branch, which follows a similar sequence of symmetry breaking bifurcations, giving rise to invariant tori with four fundamental frequencies, including resonant motions. These solutions are analysed in detail and their structure in the phase space is characterised in Sec. IV. Secondly, the investigation of chaotic attractors and the appearance of chaotic transients is performed in Sec. V. In this section, we provide numerical evidence of the existence of a crisis event destroying chaotic attractors and giving rise to chaotic transients. For a certain range of Hartmann numbers, the transients involve on-off intermittent motion, which may be due to a tangency in the phase space. Section VI contains the verification of on-off signature of these chaotic transients using standard statistical methods. Finally, Sec. VII summarises the results obtained.

II. NUMERICAL MODEL

The fluid container is a spherical shell of inner and outer radii r_i and r_o, respectively. The fluid is conducting with constant physical properties: electrical conductivity $\sigma = 1/(\eta\mu_0)$ (μ_0 is the free-space magnetic permeability), density ρ, kinematic viscosity ν, and magnetic diffusivity η. The outer sphere is kept fixed whereas the inner sphere rotates around a vertical axis with constant angular velocity Ω (see figure 1). The whole system is exposed to a uniform axial magnetic field $\mathbf{B_0} = B_0\cos(\theta)\hat{\mathbf{e}}_\mathbf{r} - B_0\sin(\theta)\hat{\mathbf{e}}_\theta$ of amplitude B_0 (θ is the colatitude).

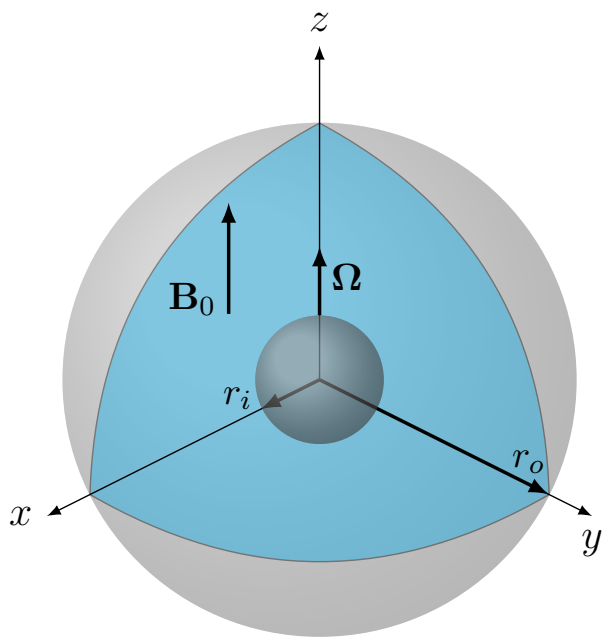

FIG. 1. Sketch of the spherical shell including the applied magnetic field and the inner sphere rotation.

To obtain a dimensionless system of equations, the characteristic quantities $d = r_o - r_i$, d^2/ν, $r_i\Omega$ and B_0 are employed as scales for length, time, velocity and magnetic field, respectively. For moderate rotation rates of the inner sphere (moderate Reynolds $\mathrm{Re} = \Omega r_i d/\nu \sim 10^3$), the inductionless approximation can be used for liquid metals, for instance, the eutectic alloy GaInSn, since the magnetic Prandtl number $\mathrm{Pm} = \nu/\eta \sim O(10^{-6})$ (Morley *et al.* (2008)) and then the requirement for a low magnetic Reynolds number $\mathrm{Rm} = \Omega r_i d/\eta = \mathrm{PmRe} \sim 10^{-3} \ll 1$ is satisfied.

In the inductionless approximation the magnetic field is decomposed as $\mathbf{B} = \hat{\mathbf{e}}_\mathbf{z} + \mathrm{Rm}\mathbf{b}$ and the terms $O(\mathrm{Rm})$ are neglected in the Navier-Stokes and induction equations

$$\partial_t \mathbf{v} + \mathrm{Re}\,(\mathbf{v}\cdot\nabla)\,\mathbf{v} = -\nabla p + \nabla^2\mathbf{v} + \mathrm{Ha}^2(\nabla\times\mathbf{b})\times\hat{\mathbf{e}}_\mathbf{z},$$
$$\nabla\times(\mathbf{v}\times\hat{\mathbf{e}}_\mathbf{z}) + \nabla^2\mathbf{b} = 0,$$
$$\nabla\cdot\mathbf{v} = 0, \quad \nabla\cdot\mathbf{b} = 0.$$

This system of equations is commonly referred to as the MSC system and depends on three parameters: the Reynolds number, the Hartmann number, and the aspect ratio

$$\mathrm{Re} = \frac{\Omega r_i d}{\nu}, \quad \mathrm{Ha} = \frac{B_0 d}{\sqrt{\mu_0\rho\nu\eta}} = B_0 d\sqrt{\frac{\sigma}{\rho\nu}}, \quad \chi = \frac{r_i}{r_o}.$$

The flow boundary conditions are no-slip ($v_r = v_\theta = v_\varphi = 0$) at the outher sphere ($r = r_o$) and constant ro-

tation ($v_r = v_\theta = 0,\ v_\varphi = \sin\theta$) at the inner sphere ($r = r_i$). Insulating exterior regions are selected for the magnetic field. This is the usual setting in previous numerical studies (e. g. Hollerbach and Skinner (2001); Garcia *et al.* (2020a)) and experiments (e. g. Kasprzyk *et al.* (2017); Ogbonna *et al.* (2020)).

The numerical method used to solve the MSC system is outlined next. A detailed description for discretisation and time stepping of the Navier-Stokes equations in rotating spherical geometry can be found in Garcia *et al.* (2010) and references therein. The velocity $\mathbf{v}$ and magnetic $\mathbf{b}$ divergence-free fields are expressed in terms of toroidal and poloidal potentials (Chandrasekhar (1981)). The expression for the velocity field is

$$\mathbf{v} = \nabla \times (\Psi \mathbf{r}) + \nabla \times \nabla \times (\Phi \mathbf{r}), \tag{1}$$

$\mathbf{r} = r\ \hat{\mathbf{e}}_\mathbf{r}$ being the position vector. The scalar potentials are expanded as spherical harmonics series (up to degree $L_{\max}$ and order $M_{\max} = L_{\max}$) in the angular coordinates (θ, φ) (φ is the longitude). In the case of the velocity potentials the spherical harmonics expansion is

$$\Psi(t, r, \theta, \varphi) = \sum_{l=0}^{L_{\max}} \sum_{m=-l}^{l} \Psi_l^m(r, t) Y_l^m(\theta, \varphi), \tag{2}$$

$$\Phi(t, r, \theta, \varphi) = \sum_{l=0}^{L_{\max}} \sum_{m=-l}^{l} \Phi_l^m(r, t) Y_l^m(\theta, \varphi), \tag{3}$$

with $Y_l^m(\theta, \varphi) = P_l^m(\cos\theta) e^{im\varphi}$, P_l^m being the normalised associated Legendre functions, of degree l and order m, satisfying $\Psi_l^{-m} = \overline{\Psi_l^m}$. The potentials are unique if the condition $\Psi_0^0 = \Phi_0^0 = 0$ is imposed. A collocation method, on a Gauss–Lobatto mesh of N_r points, is employed for the discretisation of the radial direction. OpenMP parallel strategies and optimised libraries (FFTW3, see Frigo and Johnson (2005)) and matrix-matrix products (dgemm, see Goto and van de Geijn (2008)) are implemented in the numerical code. The time integration method, based on high order implicit-explicit backward differentiation formulas (IMEX–BDF), has an explicit treatment of the Lorenz force and the nonlinear terms.

III. ANALYSIS OF MHD FLOWS

The interpretation of MHD flows is based on the analysis of very long time series obtained with direct numerical simulations (DNS) of the MSC system. The different MHD flows are computed by varying the magnetic field amplitude and keeping the rotation of the inner sphere and the aspect ratio of the shell fixed. This translates in only varying Ha and keeping the values of Re and η fixed at $\mathrm{Re} = 10^3$ and $\eta = 0.5$, respectively.

The numerical resolutions employed for this study are $n_r = 40$ radial collocation points and a spherical harmonic truncation parameter of $L_{\max} = 84$. This resolution is tested by increasing the values to $n_r = 60$ and $L_{\max} = 126$ to verify that a solution with the same temporal dependence, and with similar (within 1% of error) time-averaged properties, is obtained. Most DNS are evolved for more than 100 viscous time units to filter initial transients before the attractor is reached.

The procedure to obtain the branches of solutions is standard. A saturated solution (i. e. a solution after the initial transient) at Ha_1 is employed as initial condition for simulating the solution at $\mathrm{Ha}_2 = \mathrm{Ha}_1 + \delta\mathrm{Ha}$ (δHa may be positive or negative). The first solution is a modulated rotating wave (MRW) obtained from a rotating wave (RW) with azimuthal symmetry $m = 4$ already computed in Garcia and Stefani (2018).

We use an azimuthally constrained DNS code to compute unstable flows with certain azimuthal symmetry $m = m_1$. The only requirement is that the unstable manifold of the flow lies away from the subset $m = m_1$, i. e. the unstable mode cannot have azimuthal symmetry $m = km_1$ for any integer k. We recall that the flow has azimuthal symmetry $m = m_1$ if and only if the spherical harmonics expansion of the scalar fields (see Eq. 2) has only non-vanishing amplitudes on the azimuthal wave numbers $m = km_1$, for any integer k.

The analysis of the solutions is performed from the time series extracted from the DNS. Concretely, we analyse the volume-averaged kinetic energy

$$K = \frac{1}{2\mathcal{V}} \int_\mathcal{V} \mathbf{v} \cdot \mathbf{v}\ dv, \tag{4}$$

where $\mathcal{V}$ is the shell volume and $\mathbf{v}$ is the velocity field. We also consider the kinetic energies K_m associated with each azimuthal wave number m, obtained by only considering the spherical harmonics amplitudes Ψ_l^m and Φ_l^m of a single order $m = m_0$ and degree l satisfying $|m_0| \le l \le L_{\max}$ and setting to zero all the other amplitudes with $m \neq m_0$. The analysis of K_m for different azimuthal modes m provides information about how energy is distributed in space and helps to identify the most energetic wave number $m_{\max}$ which satisfies $\overline{K}_{m_{\max}} > \overline{K}_m$, $1 \le m \le L_{\max}$, and $m \neq m_{\max}$, with the overline representing a time average. The non-axisymmetric kinetic energy K_{na} is computed considering only the $m \neq 0$ wave numbers in the spherical harmonics expansion of the potential fields and measures the departure of the solutions from the purely axisymmetric ($m = 0$) base flow. The poloidal kinetic energy K^{P} or the non-axisymmetric toroidal kinetic energy $K_{\mathrm{na}}^{\mathrm{T}}$ are defined by only using the poloidal scalar or the $m \neq 0$ azimuthal wave numbers of the toroidal scalar, respectively, in the expression of the velocity field. While the poloidal scalar is directly related to the radial component of the velocity, the toroidal scalar only contributes to the azimuthal and colatitudinal components.

As discussed in the introductory section, the system is $\mathbf{SO}(2)\times\mathbf{Z}_2$-equivariant (invariant to azimuthal rotations and reflections with respect to the equatorial plane). These systems are associated with a particular type of solutions called rotating waves (RW) and modulated ro-

tating waves (MRW), which can be precisely defined in terms of their spatio-temporal symmetry (e. g. Rand (1982); Golubitsky, LeBlanc, and Melbourne (2000); Sánchez, Garcia, and Net (2013); Budanur *et al.* (2017); Garcia *et al.* (2019)).

A solution of the system $u(t, r, \theta, \varphi)$ is a rotating wave (RW) if $u(t, r, \theta, \varphi) = \mathcal{R}(\omega t)u(0, r, \theta, \varphi)$, where $\mathcal{R}(\omega t)$ is a rigid rotation about the vertical axis of angle ωt. Then, the RW is described as a solid body rotation at a constant angular velocity ω of a given pattern $u(0, r, \theta, \varphi)$. Although a RW is periodic, its azimuthally-averaged properties are constant. If the solution is a modulated rotating wave, $u(t, r, \theta, \varphi) = \mathcal{R}(\omega t + \gamma(t))\tilde{u}(t, r, \theta, \varphi)$, where γ and $\tilde{u}$ are τ-periodic functions of time. In this case, the temporal dependence of the solution is described by two fundamental frequencies ω and $2\pi/\tau$. Because of this particular spatio-temporal symmetry, the azimuthally-averaged properties are periodic.

Rotating waves develop once the base axisymmetric state becomes unstable to non-axisymmetric perturbations. Secondary Hopf-type bifurcations of RW give rise to MRW with two fundamental frequencies (invariant tori). Successive Hopf-type bifurcations result in MRW with three and even four fundamental frequencies as studied in Garcia *et al.* (2020b). To identify quasiperiodic MRW with N_f fundamental frequencies and azimuthal symmetry $m = m_1$, the notation N_fT-MRW$_{m_1}$ is used. These quasiperiodic flows are investigated by means of a Fourier based refined analysis (Laskar (1993b)) and Poincaré sections as will be subsequently outlined.

As commented above, the main frequency of RW and MRW, corresponding to the azimuthal drift of the wave, is removed from the frequency spectrum of volume-averaged quantities. These quantities are constant in time for RW, periodic for 2T-MRW, quasiperiodic with two fundamental frequencies for 3T-MRW, and quasiperiodic with three fundamental frequencies for 4T-MRW. For this reason the Poincaré sections of volume-averaged quantities for 2T-MRW correspond to a single point, to a closed curve for 3T-MRW , and to a surface for 4T-MRW. Poincaré sections of weakly chaotic flows (consisting of a cloud of points) may resemble surface-like sections of regular 4T-MRW. To fully distinguish both types of solutions, we have performed the chaos test of Laskar, Froeschlé, and Celletti (1992); Laskar (1993a) and studied the diffusion measure of the solution in the phase space. In addition, we have checked that the three frequencies f_1, f_2, and f_3 are fundamental, in the sense that any other frequency f_j of the spectrum of any volume-averaged kinetic energy is a linear combination of the fundamental frequencies with integer coefficients.

IV. BIFURCATION DIAGRAMS OF MRW

The time-averaged and maximum values of the non-axisymmetric kinetic energy of saturated flows at $\eta = 0.5$ and $\mathrm{Re} = 10^3$ are plotted in figure 2 versus Ha. In this

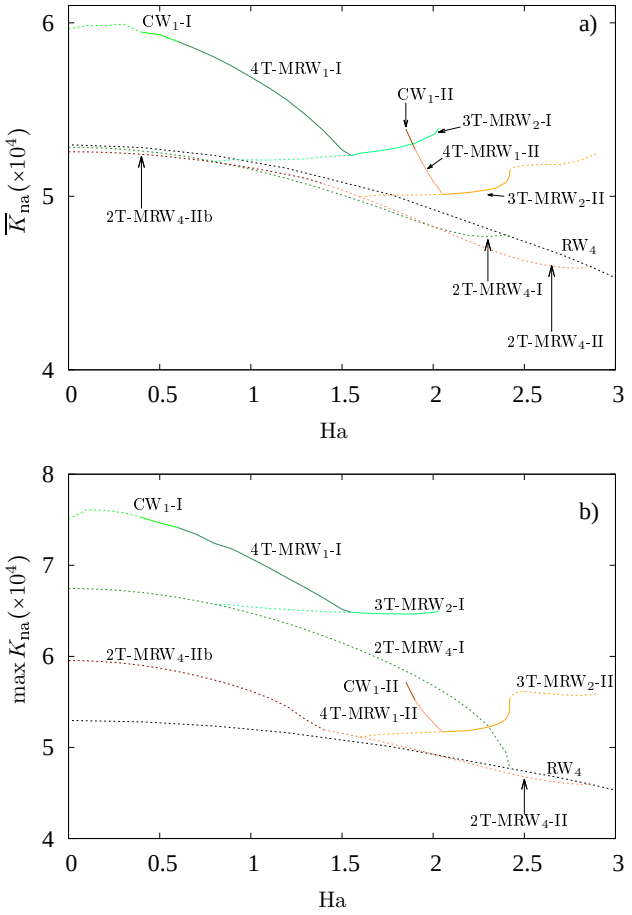

FIG. 2. Bifurcation diagram of the volume-averaged non-axisymmetric kinetic energy density K_{na} versus Ha. (a) Time-averaged K_{na} and (b) maximum values of K_{na}. Solid (dashed) lines are used for stable (unstable) flows. Branches of rotating waves RW$_m$, modulated rotating waves MRW$_m$, and chaotic waves CW$_m$, the subscript m being their azimuthal symmetry, are displayed. MRWs with N_f fundamental frequencies are labelled as N_fT, with $N_f = 2, ..., 4$. The colours distinguish the types of solutions.

figure, there are two different branches of 2T-MRW which bifurcate, without breaking the $m = 4$ symmetry, from the branch of RW with azimuthal symmetry $m = 4$ (originally computed by Garcia and Stefani (2018)). These branches are labelled as 2T-MRW$_4$-I and 2T-MRW$_4$-II. Notice that for these types of solutions, the time average is very similar to that of the parent RW$_4$ (Fig. 2(a)), but as they have oscillatory (periodic) K_{na}, the maximum value is clearly different (see Fig. 2(b)).

As described by Garcia *et al.* (2020b), for the branch I there is a sequence of Hopf bifurcations giving rise to MRW with four fundamental frequencies (branch 4T-MRW$_1$):

$$\mathrm{RW}_4 \xrightarrow{①} \text{2T-MRW}_4 \xrightarrow{②} \text{3T-MRW}_2 \xrightarrow{③} \text{4T-MRW}_1,$$

which is exactly the same sequence obtained in figure 2 for the branch II. The critical Hartmann numbers for the bifurcations on branch I are:

$$\mathrm{Ha}_1 \approx 2.4, \quad \mathrm{Ha}_2 \approx 0.8, \quad \mathrm{Ha}_3 \approx 1.52,$$

and on branch II:

$$\mathrm{Ha}_1 \approx 2.86, \quad \mathrm{Ha}_2 \approx 1.6, \quad \mathrm{Ha}_3 \approx 2.05.$$

Both sequences (I and II) of bifurcations involve the same sequence of azimuthal symmetry breaking and appearance of stable solutions:

$$\begin{array}{ccccccc} m=4 & \xrightarrow{①} & m=4 & \xrightarrow{②} & m=2 & \xrightarrow{③} & m=1 \\ \text{Unst.} & \xrightarrow{①} & \text{Unst.} & \xrightarrow{②} & \text{Unst.} & \xrightarrow{③} & \text{St.} \end{array}$$

Bifurcation ① is supercritical whereas bifurcations ② and ③ are subcritical. Although for both branches the same sequence of bifurcations occurs, their solutions have different structures in the phase space. This is shown in the next two sections, where each branch is described in detail.

A. Branch I

This branch was first studied in Garcia *et al.* (2020b), but the transition to chaotic flows (labelled as CW_1) was not clarified due to the time series, although very long (up to 100 time units), not being sufficiently long to cope with very small frequencies exhibited by some solutions along the branch of 4T-MRW_1-I (around $\mathrm{Ha} = 1.35$) as we show in the following. The power spectral density (psd) of K_4 is displayed in figure 3(a) for a 4T-MRW_1-I at $\mathrm{Ha} = 1.3$ and a detail of the lower frequencies including the psd of 4T-MRW_1-I at $\mathrm{Ha} = 1.2$ and at $\mathrm{Ha} = 1.4$ are displayed in figure 3(b). The minimum frequencies are $f_{\min} = 0.205$ for $\mathrm{Ha} = 1.2$, $f_{\min} = 0.0311$ for $\mathrm{Ha} = 1.3$, and $f_{\min} = 0.412$ for $\mathrm{Ha} = 1.4$, i. .e, the value at $\mathrm{Ha} = 1.3$ is almost an order of magnitude smaller than those at the neighbouring Ha.We have checked that the smallest frequencies of the psd correspond to $f_{\min} = 2f_3 - f_2$, where f_1, f_2, and f_3 are the fundamental frequencies labelled in fig. 3(a).

To demonstrate that the solution at $\mathrm{Ha} = 1.3$ is a regular, i. e. a 4T-MRW_1 and not a chaotic flow, the diffusion measure of the orbit in the phase space is estimated from a time dependent accurate frequency analysis following the algorithm of Laskar, Froeschlé, and Celletti (1992); Laskar (1993a), which has been successfully applied to the MSC problem in Garcia *et al.* (2021). The procedure requires the selection of a time window $T < T_f$ (T_f is the total time interval of the time series) and the computation of the first fundamental frequency f_1 using Laskar's algorithm Laskar (1993b), which achieves a relative accuracy of around 10^{-5}, over the time window T. The solution is considered regular if the variation of f_1 over the different time windows (covering the total time interval) is smaller than the considered accuracy. Figure 4(a) displays the value of f_1 versus time for different time windows $T = 10, 20, 40, 60, 100$, and a final time of $T_f = 200$. This figure clearly shows that only for $T = 60$ and $T = 100$ the variation of the frequency is insignificant. This variation is quantified in Fig 4(b) by employing the time difference $\delta f(t) = |f(t+T) - f(t)|$ which only can be computed for $t < T_f - 2T$ (see Garcia *et al.* (2021) for details). For $T = 60$, values of $\delta f(t) \approx 10^{-4}$ are obtained whereas for $T \leq 40$ (used in Garcia *et al.* (2020b)) the time difference rises to $\delta f(t) \approx 10^{-3}$. Since only time windows $T \leq 40$ over a total time interval of $T_f = 100$ were used in Garcia *et al.* (2020b), the solution was not classified as regular. With time series spanning up to $T_f = 200$, we have been able to confirm the regular character of all the solutions on branch 4T-MRW_1 down to $\mathrm{Ha} = 0.7$. With the same length of the time series, the solution obtained at $\mathrm{Ha} = 0.6$ gives rise to variations of order 10^{-2} for frequencies computed with time windows of length $T = 100$. This ensures that the solution is chaotic so the transition to chaotic flows CW_1-I may be approximated to occur at $\mathrm{Ha} \approx 0.65$.

Because f_1, f_2 and f_3 are fundamental, any other frequency f_j is a linear combination of f_1, f_2 and f_3 with integer coefficients. The relative error value for the linear combinations of the frequencies f_j is $\epsilon_j = |f_j - k_j^1 f_1 - k_j^2 f_2 - k_j^3 f_3|/f_j$. A linear combination is valid whenever $\epsilon_j < 5 \times 10^{-5}$ in accordance with the relative accuracy (10^{-5}) achieved for the frequencies (see Garcia *et al.* (2021) for a detailed study of this accuracy). We observe that as Ha is decreased along the branch the number of f_j with larger amplitudes increases so that larger integers k_i are required for the linear combinations. We have used $6 \leq k_i \leq 18$ and considered the frequencies f_j with amplitudes larger than $10^{-6} A_{\max}$, where $A_{\max}$ is the largest amplitude of the psd.

As noticed above for $\mathrm{Ha} = 1.3$, there may be linear combinations of the fundamental frequencies which become very small, and even vanish, as Ha is decreased along the branch 4T-MRW_1. This is because the fundamental frequencies vary with Ha and so do the linear combinations. When a linear combination having at least one coefficient equal to unity vanishes, a resonant solution is obtained with one less fundamental frequency. This is the case for $\mathrm{Ha} = 0.8$ where the relative error of the resonance is $\epsilon_{\mathrm{res}} = (f_1 - 4f_2 + f_3)/f_1 = 8.3 \times 10^{-8}$. For this solution the Poincaré section involving volume-averaged kinetic energies will be a closed curve. This is shown in figure 5 for the Poincaré section at the time instants t_i where $K(t_i) = 0.02177$ (recall that K is the volume-averaged kinetic energy). The volume-averaged poloidal kinetic energy $K^{\mathrm{P}}(t_i)$ is displayed versus the volume-averaged non-axisymmetric toroidal energy $K^{\mathrm{T}}_{\mathrm{na}}(t_i)$ for $\mathrm{Ha} = 0.85$ (a), $\mathrm{Ha} = 0.8$ (b), and $\mathrm{Ha} = 0.75$ (c). At $\mathrm{Ha} = 0.8$ the Poincaré section is a complicated but closed curve evidencing the resonance condition.

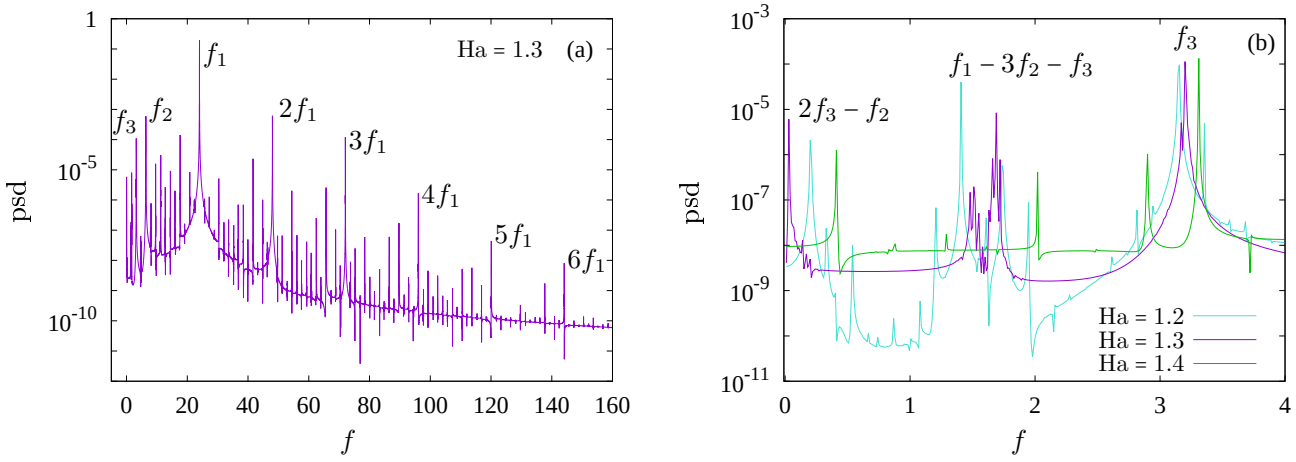

FIG. 3. **Frequencies on branch 4T-MRW$_1$-I:** (a) Power spectral density (psd) for the volume-averaged kinetic energy density K_4 of the $m = 4$ mode for the 4T-MRW$_1$ at Ha = 1.3. (b) Detail of (a) including the psd of the 4T-MRW$_1$ at Ha = 1.2 and at Ha = 1.4.

B. Branch II

As commented on before, this branch follows the same sequence of bifurcations as branch I, but an additional branch of 2T-MRW$_4$ (labelled IIb) develops from 2T-MRW$_4$-II by means of a period doubling bifurcation at Ha$_{\rm pd} \approx 1.4$ (see figure 2). Period doubling bifurcations of 2T-MRW are common in the MSC system at low Ha. They have been described by Garcia *et al.* (2020a) for flows with azimuthal symmetry $m = 2$ and $m = 3$.

At the bifurcation point ③, the solutions on the branch 3T-MRW$_2$-I become stable. The same happens for branch II. By increasing Ha from this point along the branch of 3T-MRW$_2$-I becomes unstable at around Ha $\gtrsim 2$. For Ha = 2.05 or Ha = 2.1 and by taking as the initial condition the solution at Ha = 2 on the 3T-MRW$_2$-I branch, a solution on the 3T-MRW$_2$-II is obtained after an initial transient when integrating the MSC equations with constrained azimuthal symmetry $m = 2$. As the branches 3T-MRW$_2$-I and 3T-MRW$_2$-II have $m = 2$ azimuthal symmetry, the eigenfunction at the bifurcation point (on branch I) should have at least $m = 2$ azimuthal symmetry. This gives evidence for a connection between the unstable and stable manifolds of branch 3T-MRW$_2$-I and branch 3T-MRW$_2$-II, respectively. This behaviour is not found for branch II, where unstable solutions of 3T-MRW$_2$-II, arising due to a local bifurcation at Ha$_{\rm sn} \approx 2.42$, can be integrated.

Despite the solutions on branches I and II following the same sequence of bifurcations and originating from the same branch of RW$_4$, the orbits of the solutions have significantly different distributions in the phase space, revealing different degree of complexity. Notice also that the existence of 4T-MRW$_1$-II is restricted to a small Ha interval. The three-dimensional plots of figure 7 correspond to the phase portraits of volume-averaged kinetic energies (see figure caption for details) including a Poincaré section (the grid plane) for a 3T-MRW$_2$ and a 4T-MRW$_1$ solutions on branch I (panels (a) and (c)) and on branch II (panels (b) and (d)). While the solutions on branch I have a phase portrait with a clear toroidal-like structure, the phase portraits of solutions on branch II are more folded and intricate with spherical-like shape.

In the framework of a sequence of bifurcations giving rise to 3T and 4T (high-dimensional tori) in the one dimensional nonlinear system of wave propagation of He (2005), the appearance of bursting intermittent solutions was associated with a tangency of the orbit in the phase space that allows an occasional riddling, giving rise to the intermittent behaviour. In our case this tangency has already happened on branch 3T-MRW$_1$-II at around Ha $\approx$ 2.25. This is clearly seen on figure 7 (b) for a 3T-MRW$_1$-II at Ha $\approx$ 2.1 where the two patches of the Poincaré section overlap as in He (2005).

As for branch I, the transition to chaotic flows is investigated by means of a time-dependent refined frequency analysis requiring long time integrations over 100 time units. We have estimated the critical Hartmann number for this transition to be Ha $\approx$ 1.88. Chaotic flows, either on branches I or II, are stable over a relatively small interval of Ha. For branch I they lose stability at Ha $\approx$ 0.45 and for branch II at Ha $\approx$ 1.75. By further decreasing Ha on each branch, chaotic flows become unstable giving rise to large initial transients. The sudden disappearance of a chaotic attractor as the parameter of the system is varied usually corresponds to a boundary crisis (Grebogi, Ott, and Yorke (1982)), which occurs as the chaotic attractor collide with unstable fixed points, periodic orbits, or invariant tori (Grebogi, Ott, and Yorke (1983)). By taking a look at the bifurcation diagram of branch I (fig. 2), it may be that the collision of CW$_1$-I branch occurs with the unstable 4T-MRW$_1$-I branch, born when the branch 4T-MRW$_1$-I loses stability. This could be possible since both branches may have similar values of $\overline{K_{\rm na}}$ close to the crisis. A similar situation seems to happen with branch II.

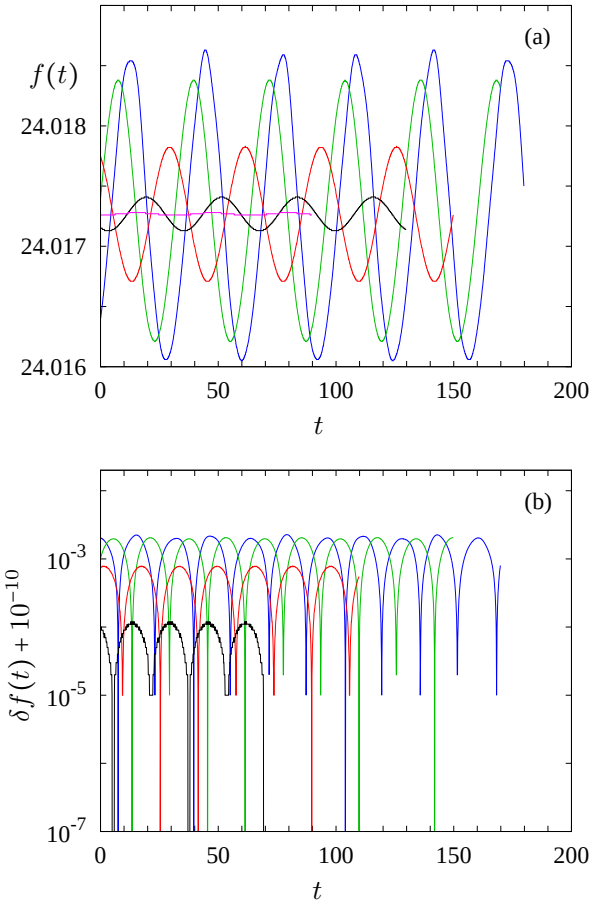

FIG. 4. **Diffusion measure on branch 4T-MRW$_1$-I:** Time-dependent frequency spectrum based on Laskar algorithm (SDDSToolKit). The time series corresponds to the volume-averaged kinetic energy of the $m = 4$ component of the flow. (a) Frequency with maximum amplitude versus time. (b) Time difference $\delta f(t) = |f(t+T) - f(t)|$ versus time (logarithmic scale). Different colors denote different lengths of the time series (blue $T = 10$, green $T = 20$, red $T = 40$, black $T = 60$, and magenta $T = 100$). The solution corresponds to a 4T-MRW$_1$ at Ha $= 1.3$ with a very small frequency peak (Fig. 3(b)).

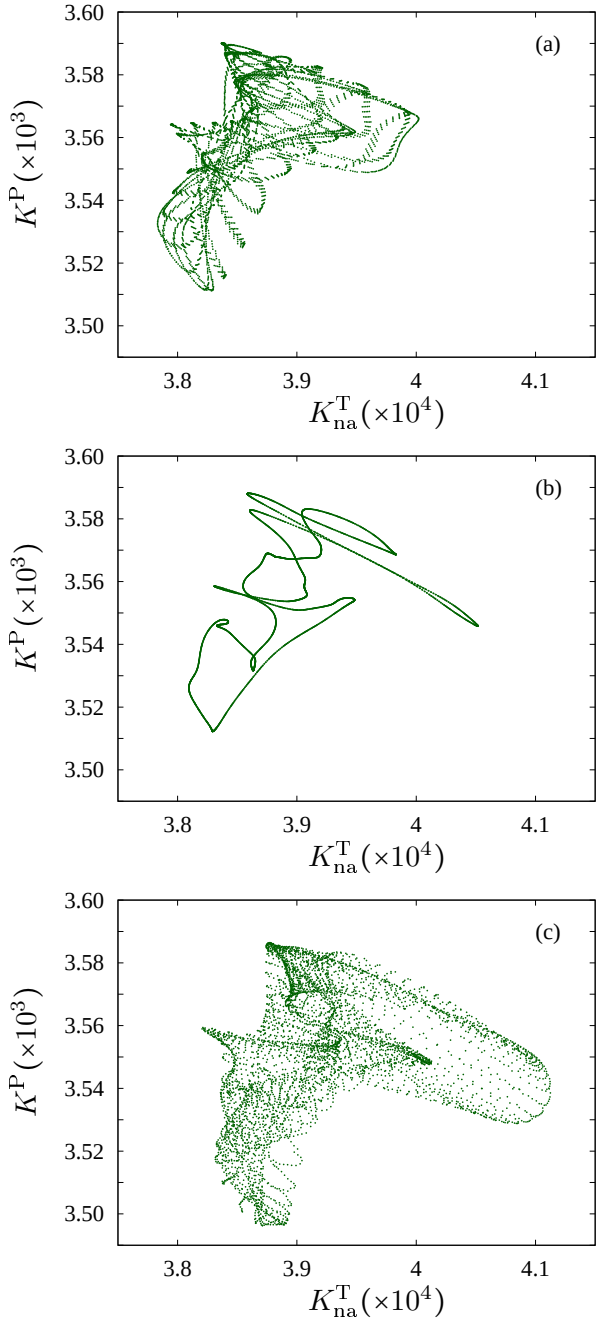

FIG. 5. **Resonances on branch 4T-MRW$_1$-I:** Poincaré sections at the time instants t_i defined by the constraint $K(t_i) = 0.02177$, K being the volume-averaged kinetic energy. The volume-averaged poloidal kinetic energy $K^{\mathrm{P}}(t_i)$ is displayed versus the volume-averaged toroidal non-axisymmetric energy $K^{\mathrm{T}}_{\mathrm{na}}(t_i)$. The solutions are 4T-MRW$_1$ at (a) Ha $=$ 0.85, (b) Ha $= 0.8$, and (c) Ha $= 0.75$.

We remark that chaotic flows may also lose stability by means of a blow-out bifurcation (Ott and Sommerer (1994)), for which the chaotic state lies within an invariant manifold. This will be the case, for instance, when the chaotic attractor has certain spatial symmetries (Ott *et al.* (1995)), which does not correspond to our situation (chaotic flows have lost all azimuthal symmetries). In addition, blow-out bifurcations may as well give rise to chaotic transients when the chaotic attractor before the bifurcation has a riddled basin of attraction. Conversely, if the basin of the chaotic attractor losing stability is not riddled, the blow-out bifurcation gives rise to intermittent behaviour (Ott and Sommerer (1994)). In our case, the situation is just the reverse. For branch II, the basin of attraction of the chaotic attractor seems to be riddled (due the tangency in the phase space), but as it is shown in the next section, we observe intermittent behaviour. For branch I, the basin of attraction is not riddled but intermittent phenomena seems not to be present. For all these reasons, we tend to believe that chaotic flows lose stability by means of a crisis and not by means of a blow-out bifurcation. Schematic diagrams summarising

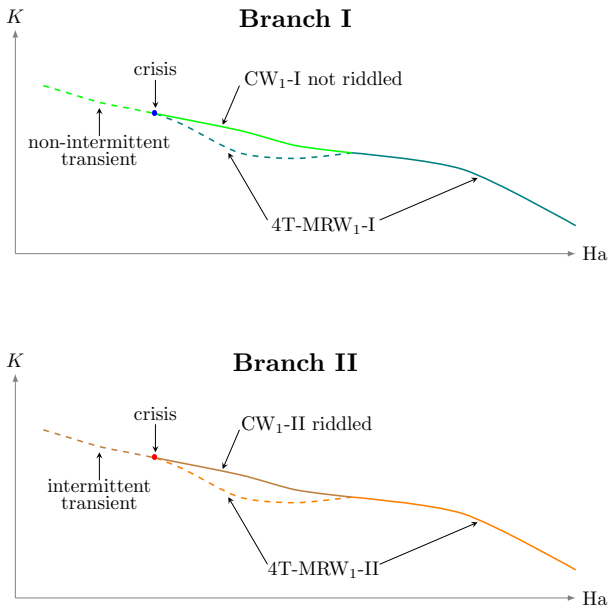

FIG. 6. **Possible crisis scenario for branches I and II:** Schemes of the bifurcation diagrams displaying a crisis event of the chaotic waves in branches I (top) and II (bottom). The difference between branch I and branch II is that chaotic waves for branch II are riddled and that the transients after the crisis display intermittent behaviour.

the possible scenarios for branches I and II are shown in Fig 6.

V. TRANSIENT BEHAVIOUR

This section is devoted to the description and analysis of initial transients, which can span long time intervals. They are sometimes found when taking initial conditions on the branches of chaotic waves CW_1-I and II. As commented in the previous section, the existence of these long initial transients seems to be related with the occurrence of a boundary crisis at which a chaotic attractor loses stability developing a chaotic saddle (Grebogi, Ott, and Yorke (1982, 1983)). The time evolution of initial conditions lying close to these chaotic saddles, which are invariant sets repelling in some directions of the phase space (Kantz and Grassberger (1985)), is characterised by a long-lived chaotic behaviour that suddenly stops and reaches a stable, usually regular attractor, afterwards. Recently, the existence of a terminal transient phase just before the appearance of the final attractor was made evident in Lilienkamp and Parlitz (2018).

The sudden disapearance of the long-lived chaotic transient behaviour and the convergence towards a regular attractor is visualised in Fig. 8. The time evolution of the kinetic energies K_m for $m = 1, .., 4$ during the transient phase close to chaotic saddles corresponding to branch I (from now on called saddles I) is displayed in Fig. 8(a) for Ha = 0. The same plot is shown in Fig. 8(b) for the transient phase close to chaotic saddles corresponding to branch II (saddles II) for Ha = 1.3. In both panels, the dominant azimuthal wave number is $m = 4$, since $K_4 \gg K_m$ $(m = 1, 2, 3)$. On average, K_4 may be more than one order of magnitude larger than K_m $(m = 1, 2, 3)$, and about two orders of magnitude larger at some intervals. For these time intervals, the transient phase almost lies in the invariant subspace $m = 4$ (i. e. it is quasi-invariant). Notice that in figure 8, the lifetime of the transient phase (i. e. the limits of the horizontal axis) varies with Ha. This lifetime also strongly depends on the initial condition considered, but statistically tends to infinity when the critical parameter of the crisis is approached (Grebogi *et al.* (1987)). The main difference between figure 8(a) and figure 8(b) is that in the latter (i. e. for the transient phases close to saddles II), the time intervals where $K_4 > 10K_m$ $(m = 1, 2, 3)$, i. e. the time intervals where the solution lies in the quasi-invariant subspace, are longer and more frequent. Nevertheless, both long-lived transients ultimately saturate to a regular solution, a 2T-MRW_3 (with $m = 3$ azimuthal symmetry) described previously in Garcia *et al.* (2020a), since $K_4, K_2, K_1 \to 0$ in Fig. 8.

As Ha is decreased, chaotic saddles may develop homoclinic or heteroclinic tangencies of their invariant manifolds, which tend to increase the fractal dimension of the saddle in a stair-case way (Lai, Życzkowski, and Grebogi (1999)), giving rise to more complex chaotic transients. Numerical evidence of this behaviour is provided later in this section. Although unstable, the investigation of these transient states is important since they may exist for very long times and thus may be the only states that can be detected experimentally. These transient states exhibit a temporal behaviour which can be related with the existence of unstable MRW belonging to branches I and II. Specifically, the transients of branch I (those occurring for Ha < 0.45) seem to sometimes approach the unstable branch of 2T-MRW_4-I, whereas the transients corresponding to branch II (those occurring for $0.9 <$ Ha < 1.7) may approach either the unstable branches 2T-MRW_4-IIb, 3T-MRW_2-I, or 3T-MRW_2-II.

Figure 9(a) displays the non-axisymmetric kinetic energy $K_{\rm na}$ versus time for the transient at Ha = 0.0 (i. e. corresponding to saddle I). The evolution of $K_{\rm na}$ seems to alternate between periods of chaotic oscillatory behaviour (marked with the (c) label) and periods of regular oscillations (marked with the (b) label). By comparing the kinetic energy of the most energetic mode (K_4) of the transient with that of an unstable 2T-MRW_4-I at Ha = 0.0 (see Fig. 9(b)) during the time interval marked with (b) in Fig. 9(a), it is clear that the transient approaches the unstable 2T-MRW_4-I, since the amplitude and period of the oscillations of K_4 are very similar. The same variables are displayed in Fig. 9(c) during a chaotic period (time interval (c) of Fig. 9(a)) of the transient together with a stable CW_1-I solution at Ha = 0.5. In

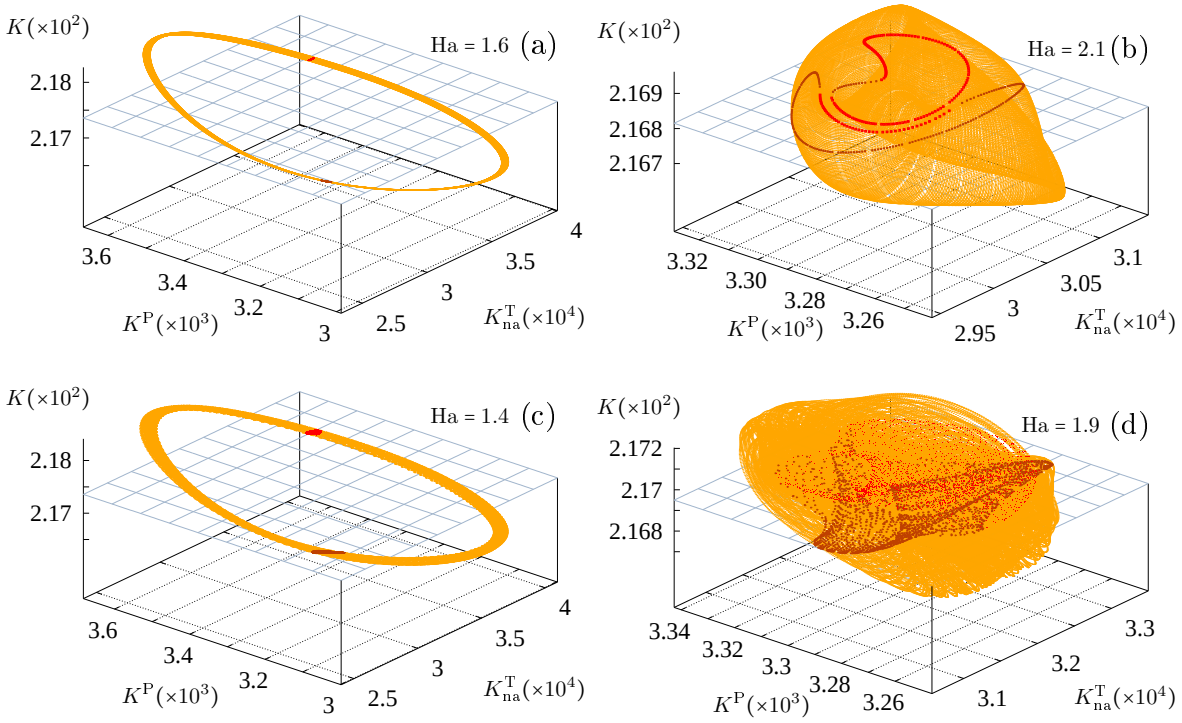

FIG. 7. **Phase space structure of branches I and II:** Phase space portraits (orange online) and Poincaré sections (brown and red online) at the time instants t_i defined by the constraint $K(t_i) = \overline{K}$, K being the volume-averaged kinetic energy and $\overline{K}$ its time average. The volume-averaged poloidal kinetic energy $K^{\mathrm{P}}(t_i)$ is displayed versus the volume-averaged toroidal non-axisymmetric energy $K^{\mathrm{T}}_{\mathrm{na}}(t_i)$ in the horizontal coordinates. (a) Solution on the 3T-MRW$_2$-I branch at Ha = 1.6. (b) Solution on the 3T-MRW$_2$-II branch at Ha = 2.1. (c) Solution on the 4T-MRW$_1$-I branch at Ha = 1.4. (d) Solution on the 4T-MRW$_1$-II branch at Ha = 1.9.

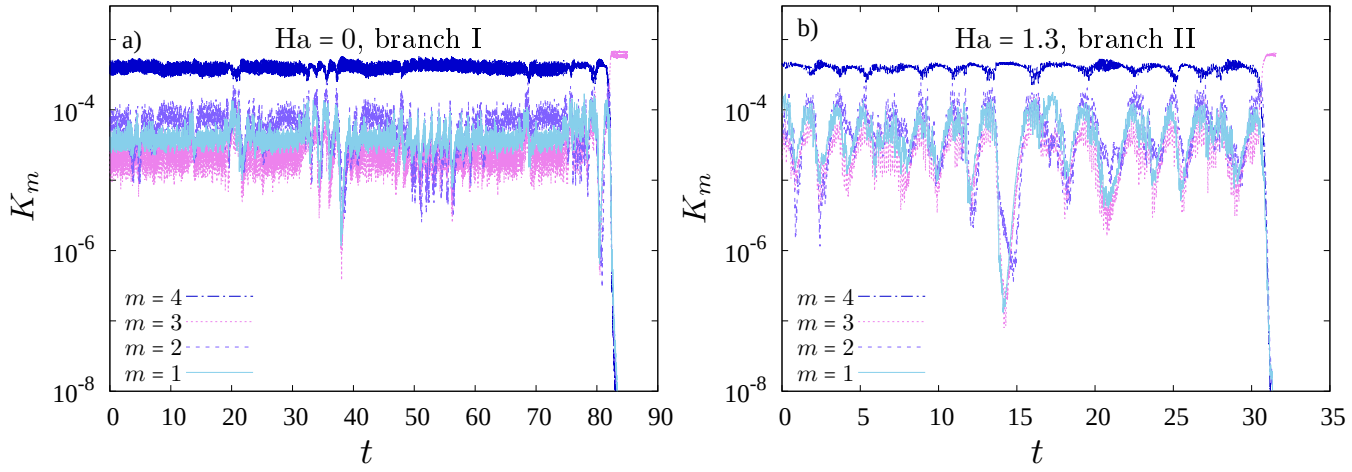

FIG. 8. **Chaotic transients from branches I and II:** Kinetic energy K_m of the azimuthal wave numbers $m = 1, 2, 3, 4$ versus time. (a) Ha = 0 corresponding to branch I. (b) Ha = 1.3 corresponding to branch II.

this case, the transient strongly resembles the chaotic attractor before the crisis. To provide further evidence of the relation between the transient and the unstable 2T-MRW$_4$-I or the chaotic attractor before the crisis, the time series of their kinetic energies of the $m = 8$ mode and that of the $m = 1$ mode are displayed in Fig. 10(a) and Fig. 10(b), respectively. The agreement between the transient time series and the other shown in the figure is as clear as in Fig. 9.

Poincaré sections of volume-averaged kinetic energies help to confirm the dynamics close to the saddle. They are defined by the constraint $K(t) = \overline{K}$, with K being the volume-averaged kinetic energy and $\overline{K}$ its time average. The volume-averaged poloidal kinetic energy

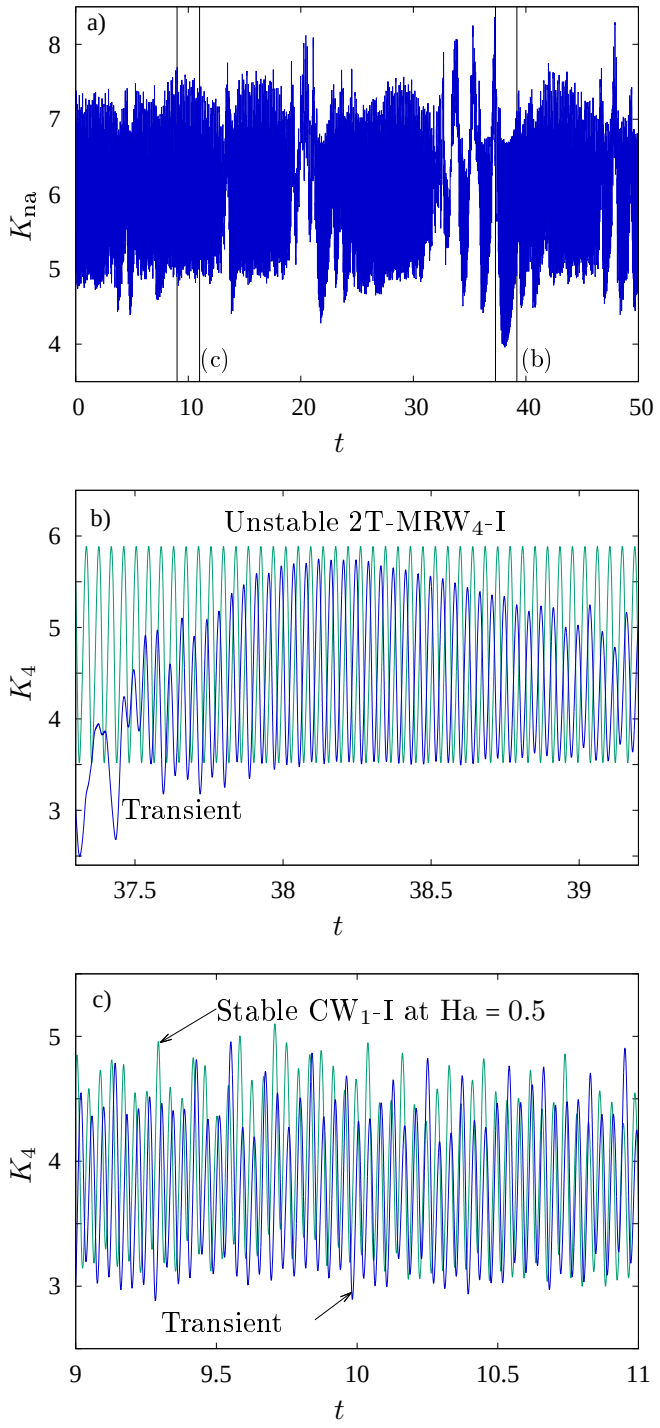

FIG. 9. **Chaotic transient at** Ha = 0.0**:** (a) Non-Axisymmetric kinetic energy , $K_{\rm na}$ versus time for the transient at Ha = 0.0. (b) Comparison between K_4 of the transient and K_4 of the unstable two tori 2T-MRW$_4$-I, both at Ha = 0.0. (c) Comparison between K_4 of the transient at Ha = 0.0 and K_4 of the stable CW$_1$ at Ha = 0.5. The time intervals of (b,c) are marked in (a).

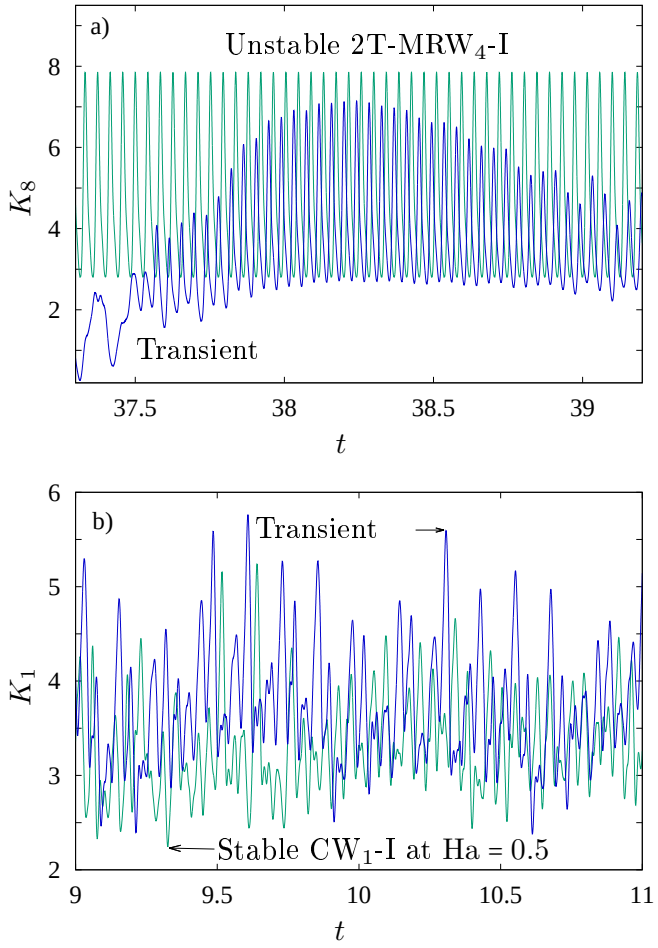

FIG. 10. **Chaotic transient at** Ha = 0.0**:** (a) Comparison between K_8 of the transient and K_8 of the unstable 2T-MRW$_4$-I, both at Ha = 0.0. (c) Comparison between K_1 of the transient at Ha = 0.0 and K_1 of the unstable CRW$_1$ at Ha = 0.5. The time intervals of (a,b) correspond to those of (b,c) in Fig. 9.

$K^{\rm P}$ is displayed versus the volume-averaged toroidal non-axisymmetric energy $K^{\rm T}_{\rm na}$ at the Poincaré sections in Fig. 11. Panel (a) contains the comparison of the transient, during the period (b) of Fig. 9, with the unstable 2T-MRW$_4$-I (the two square points) at Ha = 0.0. Although the transient points (circles) are scattered all over the plot (as they should), they tend to be concentrated very close to the square points corresponding to the Poincaré section of the 2T-MRW$_4$-I. Similarly, the pair of clouds of points (circles) of Fig. 11(b) corresponding to the transient have similar topologies and they are located over the two patches of the Poincaré section of the stable CW$_1$-I solution at Ha = 0.5.

Figures 12 and 14 are analogous to Fig. 9, but for transients at Ha = 1.3 and Ha = 1.7, respectively, associated with the chaotic saddle II. For Ha = 1.3, there are different periods of time where the solution approaches either an unstable 2T-MRW$_4$-IIb or an unstable 3T-MRW$_2$-II (both at Ha = 1.3). This is shown in Fig. 13, which

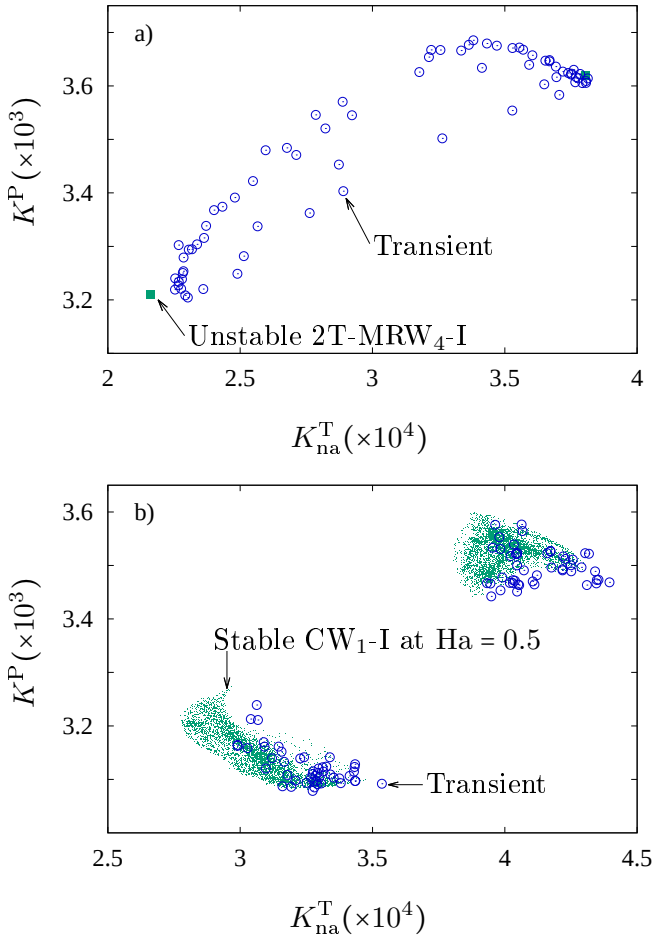

FIG. 11. **Chaotic transient at** Ha = 0.0**:** Poincaré sections defined by the constraint $K(t) = \overline{K}$, K being the volume-averaged kinetic energy and $\overline{K}$ its time average. The volume-averaged poloidal kinetic energy K^{P} is displayed versus the volume-averaged toroidal non-axisymmetric energy $K^{\mathrm{T}}_{\mathrm{na}}$. (a) Poincaré sections for the transient (restricted to the time interval (b) of Fig. 9, circles) and for the unstable 2T-MRW$_4$-I (squares), both at Ha = 0.0. (b) Poincaré sections for the transient at Ha = 0.0 (restricted to the time interval (c) of Fig. 9, circles) and for the stable CRW$_1$ at Ha = 0.5 (dots). Because volume-averaged properties are considered, the Poincaré sections of 2T are a single point.

compares the contour plots of the radial velocity of the transient at some time instants with the corresponding contour plots of the unstable 2T-MRW$_4$-IIb or the unstable 3T-MRW$_2$-II, both at Ha = 1.3. In Fig. 12(b), the period doubling giving rise to the unstable 2T-MRW$_4$-IIb branch is also reproduced during the transient phase. For the transient at Ha = 1.7, besides the periods approaching the 3T-MRW$_2$-II (fig. 14(b)), there are periods reminiscent of the chaotic attractor before the crisis (fig. 14(c)). Notice that in this case, the transient neither can approach the branch of 2T-MRW$_4$-IIb or 3T-MRW$_2$-I since these branches are born at Ha < 1.6.

Figure 14(a) seems to display oscillatory regular behaviour for approximately $t \in [15, 20]$, just before the time period marked with the label (b), i. e. before the transient approaches the unstable 3T-MRW$_2$-II branch. In addition, for $t \in [15, 20]$, the transient at Ha = 1.7 has a symmetry of nearly $m = 2$. This may be an indication that the transient is approaching the branch 3T-MRW$_2$-I as we argue in the following. As commented in Sec. IV B, the unstable invariant manifold of branch 3T-MRW$_2$-I seems to be connected with the stable invariant manifold of branch 3T-MRW$_2$-II at around Ha ≈ 2, where the branch 3T-MRW$_2$-I loses stability, seemingly by means of a saddle-node bifurcation. This is because taking an initial condition on branch 3T-MRW$_2$-I and integrating with Ha > 2, a solution on the branch 3T-MRW$_2$-II is reached. The unstable part of 3T-MRW$_2$-I, born at the saddle node, may extend for smaller Ha = 1.7, and thus the transients close to the chaotic saddle may approach this branch and be repelled afterwards to branch 3T-MRW$_2$-II, thanks to the connection of their invariant manifolds. Aside from $t \in [15, 20]$, the approach of the transient to branch 3T-MRW$_2$-I and the subsequent repelling to branch 3T-MRW$_2$-II can be also identified from $t \in [40, 44]$.

As in Fig. 11, the Poincaré sections of volume-averaged kinetic energies are displayed in Fig. 15 and Fig. 16 for the transients found at Ha = 1.3 and Ha = 1.7, respectively, corresponding to the chaotic saddle II. The four square points of Fig. 15(a) correspond to the unstable 2T-MRW$_4$-IIb with period doubled and are surrounded by four patches of circle points corresponding to the transient during the time interval labelled with (b) in Fig. 12(b). Analogously, the circles corresponding to the transient sections, during the time interval labelled with (c) in Fig. 12(c), are located very close to the two closed curves (which can be barely distinguished) of Fig. 15(b). The similarity between the Poincaré sections of the transient and the unstable objects is repeated for Ha = 1.7 (see Fig. 16). In this case, the sections for the unstable 3T-MRW$_2$-II are clearly two closed curves, lying very close (see Fig. 16(a)). We recall (as commented in Sec. IV B) that by increasing Ha along branch 3T-MRW$_2$-II the two closed curves overlap, giving rise to a tangency of the orbit in the phase space. The overlapping of the two patches of the Poincaré section is large for the chaotic attractor of CW$_1$-II at Ha = 1.8 since these chaotic flows bifurcate from the branch 4T-MRW$_1$-II, for which the overlapping of the section already occurs. Accordingly, the overlapping of the transient at Ha = 1.7 is also large (see Fig. 16(b)).

The overlapping of the Poincaré sections may indicate a riddled basin of attraction (Sommerer and Ott (1993); He (2005)), which may favour intermittent behaviour for transients corresponding to chaotic saddles emanating from branch II. This overlapping is not present on branch I (e. g. see Fig. 7(a,c)), thereby perhaps inhibiting intermittency during the transients of chaotic saddles I. As shown in the next section, the intermittent nature of the transients corresponding to branch II is confirmed.

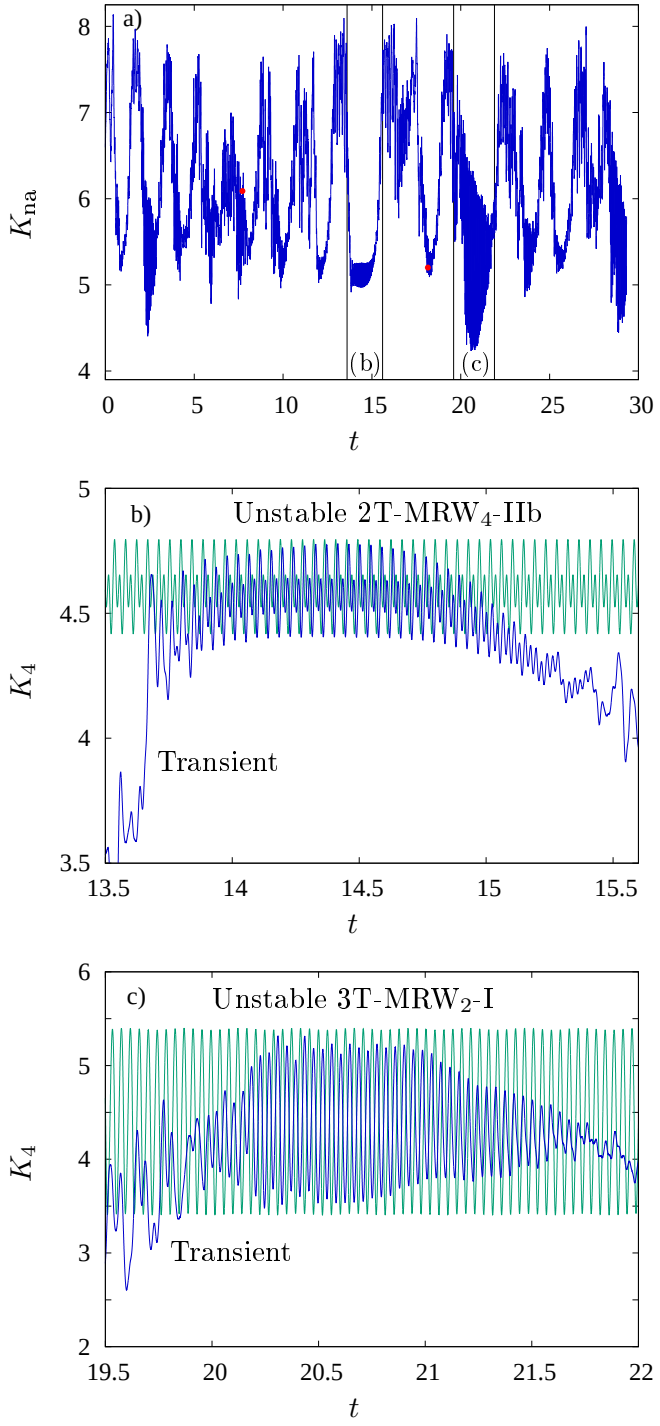

FIG. 12. **Chaotic transient at** Ha = 1.3**:** (a) Non-axisymmetric kinetic energy , $K_{\rm na}$ versus time for the transient at Ha = 1.3. The points (red online) correspond to the snapshots of Fig. 13 (b) Comparison of K_4 for the transient and the unstable 2T-MRW$_4$-IIb on a time interval indicated in (a). (c) Comparison of K_4 for the transient and the unstable 3T-MRW$_2$-I on a time interval indicated in (a).

VI. ON-OFF INTERMITTENCY STATISTICS

The previous section has provided evidence that the transients within the chaotic saddle II exhibit intermittent behaviour. During some time intervals, these transients have values of kinetic energy of the modes $m \neq 4k$ significantly smaller than those corresponding to the kinetic energy of the modes $m = 4k$, for some integer k (see Fig. 8(b)). This basically means that during these time intervals, the transient almost lies within the invariant manifold defined by the azimuthal symmetry $m = 4$ and is derailed from this manifold when the kinetic energies of the mode $m = 1, 2, 3$ are significant. This type of intermittent behaviour, in which the orbit is subsequently directed and repelled from certain unstable attractors lying within a invariant manifold (also quasi-invariant), has been defined by Platt, Spiegel, and Tresser (1993) as on-off intermittency. This type of intermittent chaos has been widely characterised (e. g. Heagy, Platt, and Hammel (1994); Platt, Hammel, and Heagy (1994); Aumaître, Pétrélis, and Kirone (2005)) and their statistical signature can be extracted from time series (e. g. Venkataramani *et al.* (1995, 1996); Toniolo, Provenzale, and Spiegel (2002)).

In this section, some statistical analyses are performed on the time series of transients close to either the chaotic saddle I (at Ha = 0.0) or the chaotic saddle II (at Ha = 0.9, 1.3, 1.7), but also to the time series of a stable chaotic attractor on branch CW$_1$-II (at Ha = 1.8). The analyses are done for $K_* = K_1 + K_2 + K_3$ as a measure of the departure of the intermittent transient from the invariant subspace of azimuthal symmetry $m = 4$. Similar results are obtained when $K_* = K_i$ and $i = 1, 2, 3$. For on-off intermittency, the probability measuring the departure from the invariant manifold should have a power law distribution $P(K_*) \sim K_*^{\gamma}$ with $\gamma \in (-1, 0)$ (Venkataramani *et al.* (1996); Toniolo, Provenzale, and Spiegel (2002)). Figure 17 displays the probability distribution function (pdf) of the kinetic energy K_* of the modes $m = 1, 2, 3, 4$ and the sum of the kinetic energies of the modes $m = 1, 2, 3$ ($K_* = K_1 + K_2 + K_3$) for the transient at Ha = 0.9. Either for $K_* = K_i$, $i = 1, 2, 3$, or for $K_* = K_1 + K_2 + K_3$, there is an interval of K_* values for which the pdf has a slope $\gamma \in (-1, 0)$, which is a signature of on-off intermittency for the transient at Ha = 0.9. This is clearly not the case for $m = 4$ since K_4 does not measure the departure from the invariant manifold, which is defined by the $m = 4$ azimuthal symmetry.

Figure 18(a) displays the pdf of $K_* = K_1 + K_2 + K_3$ for all the time series considered: a transient within the chaotic saddle I (Ha = 0.0), transients close to the chaotic saddle II (Ha = 0.9, 1.3, 1.7), and a stable solution from branch CW$_1$-II (Ha = 1.8). While for Ha = 0.9, 1.3, 1.7 (i. e. transients within the chaotic saddle II) the pdf seems to follow the predicted power laws for on-off intermittency, these can not be identified in the pdf of either the transient close to the chaotic saddle I or the stable CW$_1$-II, suggesting that these two cases do not

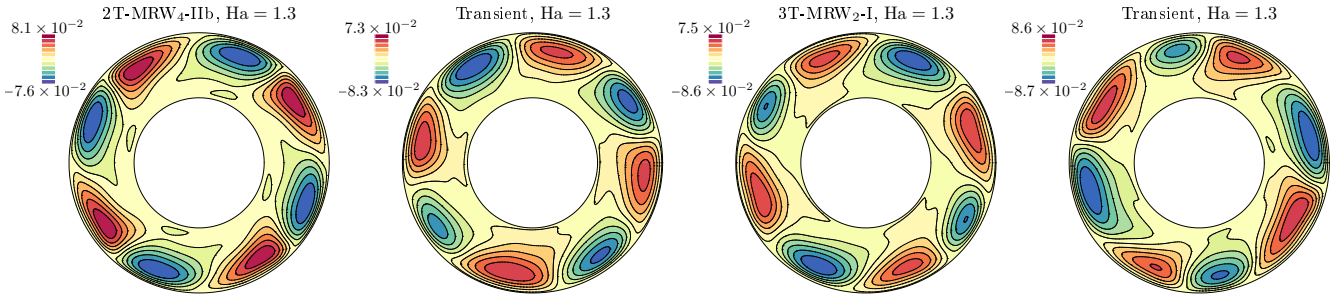

FIG. 13. **Chaotic transient at** Ha = 1.3**:** Snapshots showing the contour plots of the radial velocity on a colatitudinal slice slightly above the equator. From left to right the contour plots correspond to the unstable 2T-MRW$_4$-IIb at Ha = 1.3, the transient at Ha = 1.3 (point on the right of Fig. 12(a)) with almost $m = 4$ azimuthal symmetry, the unstable 3T-MRW$_2$-I, and the transient at Ha = 1.3 (point on the left of Fig. 12(a)) with almost $m = 2$ azimuthal symmetry, respectively.

correspond to on-off intermittency. This seems also to be confirmed with other on-off intermittency statistical indicators explained as follows.

With time series analysis, a threshold $K_c = \alpha \max K_*$, with $\alpha \sim O(0.1)$, is considered to distinguish between the on and off phases. This threshold defines the set of burst times as the times when the curve of K_* crosses the threshold line in the upper direction so the solution is away from the $m = 4$ invariant subspace (see Venkataramani *et al.* (1996)). The factors α for Ha = 0, Ha = 0.9, Ha = 1.3, Ha = 1.7, and Ha = 1.8, are $\alpha = 0.25$, $\alpha = 0.26$, $\alpha = 0.4$, $\alpha = 0.28$, and $\alpha = 0.34$, respectively, and the maximum values are $\max K_* = 4 \times 10^{-4}$, $\max K_* = 4.7 \times 10^{-4}$, $\max K_* = 4.51 \times 10^{-4}$, $\max K_* = 3.56 \times 10^{-4}$, and $\max K_* = 2.08 \times 10^{-4}$, respectively. The set of burst times (normalised) has a fractal box-counting dimension $d = 1/2$ (Venkataramani *et al.* (1996)), i. e. the number N of time intervals of length δt required to cover the fractal set follows $N(\delta t) \sim \delta t^{-1/2}$. This is displayed in Figure 18(b) and the agreement with the on-off intermittency theoretical scaling is again only valid for Ha = 0.9, 1.3, 1.7 (i. e. for transients close to the chaotic saddle II).

Another characteristic signature of on-off intermittency is provided by the notion of the set of interburst times (defined as the difference Δt of two successive burst times). The pdf of the interburst times follows the scaling $P(\Delta t) \sim \Delta t^{-3/2}$ (Venkataramani *et al.* (1996)). Figure 18(c) displays these pdf for the analysed time series. For Ha = 0.9, 1.3, 1.7 (especially for Ha = 1.3) the pdf seem to approach the valid scaling for on-off intermittent behaviour. Notice that the agreement with the theory is not clear as in Fig. 18(b) since very large time series are required to approximate the set of interburst times and the time series are limited by the lifetime of the transients. The same shortcoming occurs when considering the power spectral density (psd) of the time series of K_*. In the case of on-off intermittent signal, the psd scales as $f^{-1/2}$ (Venkataramani *et al.* (1995)), which can not be clearly identified from our time series (see figure 18(d)).

VII. CONCLUSIONS

The study focuses on the analysis of bifurcation phenomena between regular and chaotic magnetohydrodynamic (MHD) flows. These flows are obtained by direct numerical simulations of the magnetised spherical Couette (MSC) system, a widely used three-dimensional MHD model for the study of astrophysical phenomena. As recently found by Garcia *et al.* (2020b), symmetry breaking Hopf bifurcations may give rise to stable attractors described by four fundamental frequencies (i. e. four-dimensional invariant tori). According to Newhouse, Ruelle, and Takens (1978), this scenario is not possible when the system is generic (i. e. without any prescribed symmetry) since any perturbation applied to three-dimensional invariant tori gives rise to chaotic behaviour. The analysis of spatially symmetric systems, as the MSC system, is thus of fundamental importance to understand the type of bifurcations that may occur.

The mechanism, first described in Garcia *et al.* (2020b), of the generation of four-dimensional invariant tori (4T) in the form of modulated rotating waves (MRW) is confirmed in the present study by analysing a new branch of solutions. As in Garcia *et al.* (2020b), the bifurcation parameter is the Hartmann number, measuring the strength of the magnetic field applied to the system, while the other parameters (the Reynolds number and aspect ratio of the shell) are fixed. The results show that the new branch (branch II) giving rise to 4T follows the same sequence of Hopf bifurcations as the branch described in Garcia *et al.* (2020b) (branch I), but in contrast, the structure of solutions in the phase space is significantly different for both branches. By analysing Poincaré sections of 3T-MRW and 4T-MRW on both branches, we have revealed the different phase space distributions of their solutions. In the case of branch II, the two patches of the Poincaré sections overlap, indicating a tangency of the orbit (He (2005)), which may indicate a riddled basin of attraction. In contrast to this, the two patches of the Poincaré sections of solutions along branch I are clearly separated and the three-dimensional phase space plots of the orbit have a toroidal-like structure.

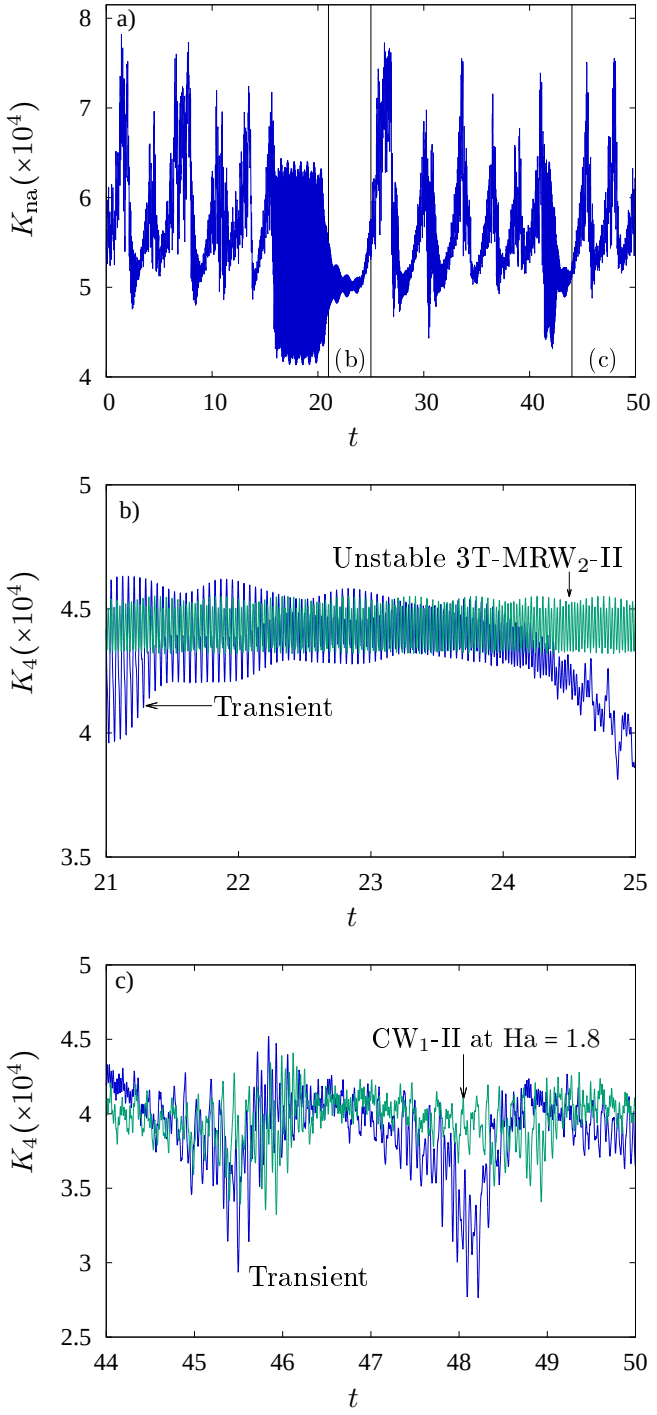

FIG. 14. **Chaotic transient at** Ha = 1.7**:** (a) Non-axisymmetric kinetic energy , K_{na} versus time for the transient at Ha = 1.7. (b) Comparison of K_4 for the transient and the unstable 3T-MRW$_2$-II on a time interval indicated in (a). (c) Comparison of K_4 for the transient and the stable CW$_1$-II at Ha = 1.8 on a time interval indicated in (a).

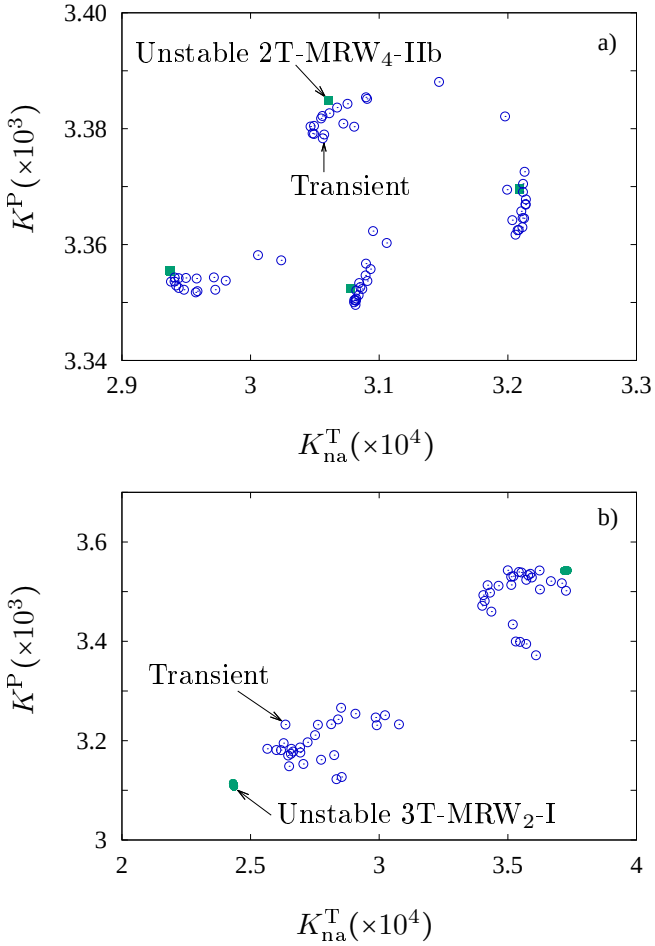

FIG. 15. **Chaotic transient at** Ha = 1.3**:** Poincaré sections defined by the constraint $K(t) = \overline{K}$, K being the volume-averaged kinetic energy and $\overline{K}$ its time average. The volume-averaged poloidal kinetic energy $K^{\rm P}$ is displayed versus the volume-averaged toroidal non-axisymmetric energy $K^{\rm T}_{\rm na}$. (a) Poincaré sections for the transient (restricted to the time interval (b) of Fig. 12, circles) and for the unstable 2T-MRW$_4$-IIb (squares). (b) Poincaré sections for the transient (restricted to the time interval (c) of Fig. 12, circles) and for the unstable three tori 3T-MRW$_2$-I (full circle). Because volume-averaged properties are considered, the Poincaré sections of 2T and 3T are a single point and a closed curve, respectively. The closed curve in (b) is so small that looks like a point, but it is not.

With the help of very long time series, we have been able to determine the transition between 4T-MRW and chaotic flows by analysing the diffusion of the orbit in the phase space following the procedure described by Laskar, Froeschlé, and Celletti (1992); Laskar (1993a). This was not possible in Garcia *et al.* (2020b) because the analysed time series were not long enough. We have shown that before the transition, 4T-MRW may develop resonances, i. e. one of the fundamental frequencies can be expressed as linear combination of the others. This is verified by employing an accurate algorithm (Laskar (1993b)) for determining the fundamental frequencies.

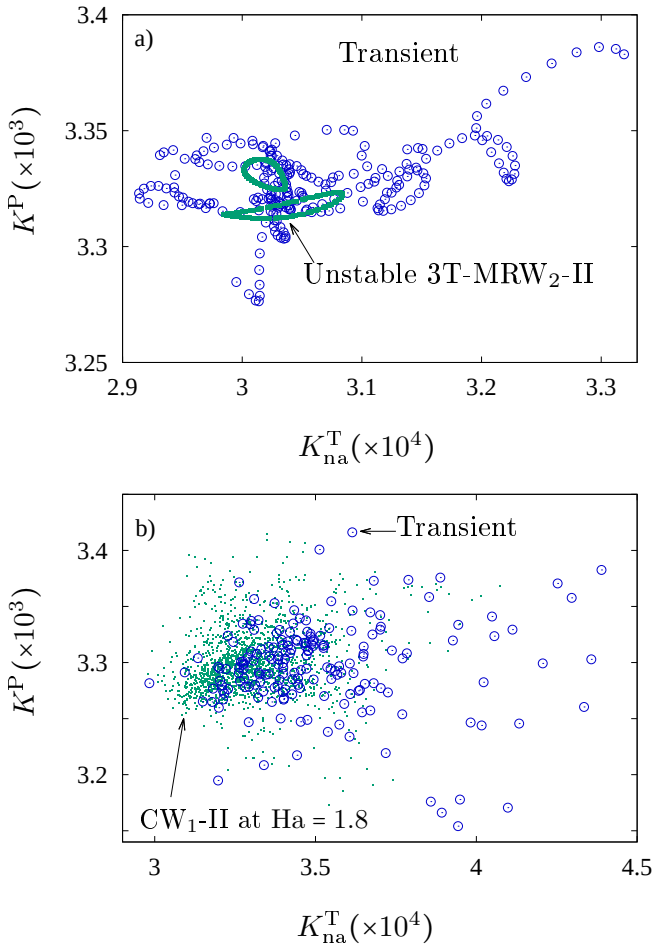

FIG. 16. **Chaotic transient at** Ha = 1.7**:** Poincaré sections defined by the constraint $K(t) = \overline{K}$, K being the volume-averaged kinetic energy and $\overline{K}$ its time average. The volume-averaged poloidal kinetic energy K^{P} is displayed versus the volume-averaged toroidal non-axisymmetric energy $K^{\mathrm{T}}_{\mathrm{na}}$. (a) Poincaré sections for the transient (restricted to the time interval (b) of Fig. 14, circles) and for the unstable 3T-MRW$_2$-II (full circle). (c) Poincaré sections for the transient (restricted to the time interval (c) of Fig. 14, circles) and for the stable CW$_1$-II (dots) at Ha = 1.8. Because volume-averaged properties are considered, the Poincaré sections of a 3T are a closed curve.

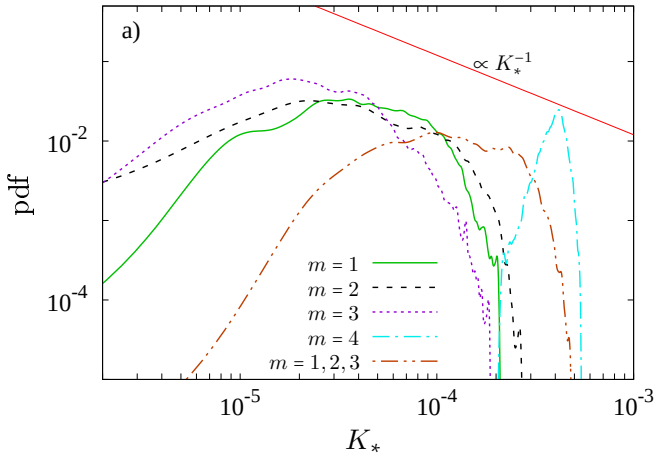

FIG. 17. Probability distribution function of the kinetic energy K_* of the individual modes $m = 1, 2, 3, 4$ for a intermittent transient flow at Ha = 0.9. For $m = 1, 2, 3$ there is a range of K_* for which the pdf has slope $\gamma \in (-1, 0)$. This is not the case for $m = 4$. The theoretical scaling is marked with a solid line (red online).

Aside from the study of high dimensional invariant tori and their transition to chaos on branches I and II, another important goal of this research is to investigate in detail the nature and prevalence of chaotic flows when varying the Hartmann number. Chaotic MHD attractors only appear to be stable in a small range of Hartmann numbers close to the transition from regular 4T-MRW. Away from the range of stability of chaotic attractors on both branches (I and II), the time integrations typically involve very long initial transients (which may exceed 50 dimensionless units) before a stable attractor (which may not belong to branch I nor branch II) is reached. The existence of these long initial transients has been interpreted as a result of a crisis, at which a stable chaotic attractor loses stability developing a chaotic saddle.

By a direct comparison of time series of volume-averaged kinetic energies and Poincaré sections of the initial transients with unstable MRW with either azimuthal symmetry $m = 4$ or $m = 2$, existing at the same parameters, we have demonstrated that during the transients, the phase space trajectory approaches these unstable MRW at certain periods, but after some time interval it is repelled farther away. The different phase space structure of unstable MRW belonging to branch I and branch II make the corresponding transients also different. Specifically, the tangency in the phase space observed for 3T-MRW belonging to branch II favours the development of intermittent behaviour (e. g. He (2005)), which is observed during the transients associated with the chaotic saddle of branch II, but not during the transients associated with branch I.

The intermittent nature of the transients is investigated by employing well-known statistical methods, including the analysis of the set of burst times, designed for the time series. In the case of transients associated with chaotic saddles of branch II, the intermittency is of on-off type whereas this is not the case for transients associated with branch I as commented earlier. On-off intermittency involves the existence of an invariant manifold, at which the intermittent trajectory is attracted, with some unstable transverse direction, from which the trajectory is subsequently repelled. In our case the on-off invariant manifold corresponds to the azimuthal symmetry $m = 4$.

On-off intermittency may arise from a blow-out bifurcation (Ott and Sommerer (1994)), but as commented in Sec. IV B, this seems to not be the case. In our situation, the existence of a riddled basin of attraction for the chaotic flows on branch II and the intricate structure of

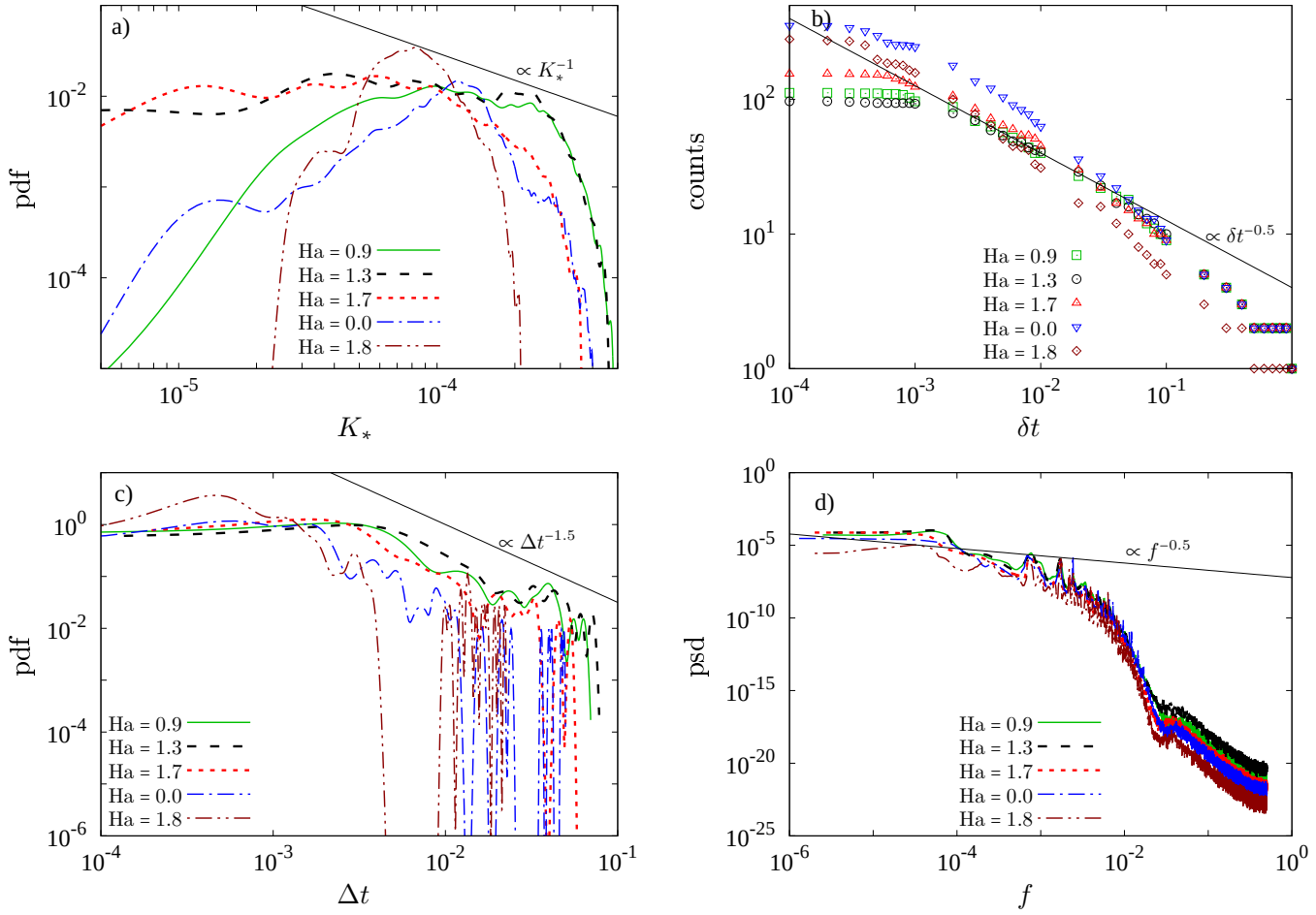

FIG. 18. (a) Probability distribution function of the sum of the kinetic energies K_* contained in the modes $m = 1, 2, 3$ for intermittent transient flows. For Ha $= 0.9, 1.3, 1.7$ there is a range of K_* for which the pdf has slope $\gamma \in (-1, 0)$. This is not the case for Ha $= 0$ or Ha $= 1.8$. (b) Number of counts versus length of the interval for the set of burst times. (c) Probability distribution function of the interburst times (d) Power spectral density of K_*. The theoretical scalings are marked with a solid straight line.

the invariant manifolds of the unstable 3T-MRW$_2$-I and 3T-MRW$_2$-II branches for Ha $\in [0.9, 1.7]$ allow the transient orbit to jump and approach the different branches, thus explaining the observed on-off intermittent signature for transients corresponding to chaotic saddle II. Conversely, the absence of this riddled basin or connection between branches I and II may also explain why the on-off intermittent signature is not found for transients within the chaotic saddle I.

Blow-out bifurcations have been found to be the mechanism for on-off intermittent dynamics in the case of MHD problems involving the emergence of dynamo action in a three-dimensional periodic box (Sweet *et al.* (2001); Alexakis and Ponty (2008)) and also in spherical geometries as is the case of Raynaud and Dormy (2013), which considers the same problem considered here but without the inductionless approximation. In these studies, the invariant manifold giving rise to the on-off intermittent behaviour corresponds to the absence of magnetic field, which is in contrast to our study since our manifold is defined in terms of the azimuthal symmetry of both velocity and magnetic fields. This is natural since in our case a magnetic field is always present, although it is very weak since the range of Hartmann numbers investigated is order of unity.

ACKNOWLEDGMENTS

This project has received funding from the European Research Council (ERC) under the European Union's Horizon 2020 research and innovation programme (grant agreement No 787544).

Alexakis, A. and Ponty, Y., "Effect of the lorentz force on on-off dynamo intermittency," Phys. Rev. E **77**, 056308 (2008).

Aumaître, S., Pétrélis, F., and Kirone, M., "Low-frequency noise controls on-off intermittency of bifurcating systems," Phys. Rev. Lett. **95**, 064101–1–4 (2005).

Avila, M. and Hof, B., "Nature of laminar-turbulence intermittency in shear flows," Phys. Rev. E **87**, 063012 (2013).

Barik, A., Triana, S. A., Hoff, M., and Wicht, J., "Triadic resonances in the wide-gap spherical Couette system," J. Fluid Mech. **843**, 211–243 (2018).

Budanur, N. B., Dogra, A. S., and Hof, B., "Geometry of transient chaos in streamwise-localized pipe flow turbulence," Phys. Rev. Fluids **4**, 102401 (2019).

Budanur, N. B., Short, K. Y., Farazmand, M., Willis, A. P., and Cvitanović, P., "Relative periodic orbits form the backbone of turbulent pipe flow," J. Fluid Mech. **833**, 274–301 (2017).

Casas, P. S. and Jorba, A., "Hopf bifurcations to quasi-periodic solutions for the two-dimensional plane Poiseuille flow," Commun. Nonlinear Sci. Numer. Simul. **17**, 2864–2882 (2012).

Chandrasekhar, S., *Hydrodynamic and Hydromagnetic Stability* (Dover publications, inc. New York, 1981).

Cherubini, S. and De Palma, P., "Nonlinear optimal perturbations in a couette flow: bursting and transition," J. Fluid Mech. **716**, 251–279 (2013).

Crawford, J. D. and Knobloch, E., "Symmetry and symmetry-breaking bifurcations in fluid dynamics," Annu. Rev. Fluid Mech. **23**, 341–387 (1991).

Dijkstra, H. A., Wubs, F. W., Cliffe, A. K., Doedel, E., Dragomirescu, I. F., Eckhardt, B., Gelfat, A. Y., Hazel, A. L., Lucarini, V., Salinger, A. G., Phipps, E. T., Sánchez-Umbría, J., Schuttelaars, H., Tuckerman, L. S., and Thiele, U., "Numerical bifurcation methods and their application to fluid dynamics: Analysis beyond simulation," Commun. Comput. Phys. **15**, 1–45 (2014).

Ecke, R. E., Zhong, F., and Knobloch, E., "Hopf bifurcation with broken reflection symmetry in rotating Rayleigh-Bénard convection," Europhys. Lett. **19**, 177–182 (1992).

Eckhardt, B., Faisst, H., Schmiegel, A., and Schneider, T. M., "Dynamical systems and the transition to turbulence in linearly stable shear flows," Phil. Trans. R. Soc. Lond. A **366**, 1297–1315 (2008).

Feng, J., "Analysis of chaotic saddles in a nonlinear vibro-impact system," Commun. Nonlinear Sci. Numer. Simul. **48**, 39–50 (2017).

Fleurantin, E. and James, J., "Resonant tori, transport barriers, and chaos in a vector field with a neimark–sacker bifurcation," Commun. Nonlinear Sci. Numer. Simul. **85**, 105226 (2020).

Frigo, M. and Johnson, S. G., "The design and implementation of FFTW3," Proceedings of the IEEE **93**, 216–231 (2005), special issue on "Program Generation, Optimization, and Platform Adaptation".

Gailitis, A., Lielausis, O., Platacis, E., Gerbeth, G., and Stefani, F., "Colloquium: Laboratory experiments on hydromagnetic dynamos," Rev. Mod. Phys. **74**, 973–990 (2002).

Garcia, F., Net, M., García-Archilla, B., and Sánchez, J., "A comparison of high-order time integrators for thermal convection in rotating spherical shells," J. Comput. Phys. **229**, 7997–8010 (2010).

Garcia, F., Seilmayer, M., Giesecke, A., and Stefani, F., "Modulated rotating waves in the magnetized spherical Couette system," J. Nonlinear Sci. **29**, 2735–2759 (2019).

Garcia, F., Seilmayer, M., Giesecke, A., and Stefani, F., "Chaotic wave dynamics in weakly magnetised spherical Couette flows," Chaos **30**, 043116 (2020a).

Garcia, F., Seilmayer, M., Giesecke, A., and Stefani, F., "Four-frequency solution in a magnetohydrodynamic Couette flow as a consequence of azimuthal symmetry breaking," Phys. Rev. Lett. **125**, 264501 (2020b).

Garcia, F., Seilmayer, M., Giesecke, A., and Stefani, F., "Long term time dependent frequency analysis of chaotic waves in the weakly magnetised spherical Couette system," Physica D **418**, 132836 (2021).

Garcia, F. and Stefani, F., "Continuation and stability of rotating waves in the magnetized spherical Couette system: Secondary transitions and multistability," Proc. R. Soc. A **474**, 20180281 (2018).

Gibson, J. F., Halcrow, J., and Cvitanović, P., "Visualizing the geometry of state space in plane couette flow," J. Fluid Mech. **611**, 107–130 (2008).

Gissinger, C., Ji, H., and Goodman, J., "Instabilities in magnetized spherical Couette flow," Phys. Rev. E **84**, 026308 (2011).

Golubitsky, M., LeBlanc, V. G., and Melbourne, I., "Hopf bifurcation from rotating waves and patterns in physical space," J. Nonlinear Sci. **10**, 69–101 (2000).

Golubitsky, M. and Stewart, I., *The Symmetry Perspective: From Equilibrium to Chaos in Phase Space and Physical Space.* (Birkhäuser, Basel, 2003).

Goto, K. and van de Geijn, R. A., "Anatomy of high-performance matrix multiplication," ACM Trans. Math. Softw. **34**, 1–25 (2008).

Grebogi, C., Ott, E., Romeiras, F., and Yorke, J. A., "Critical exponents for crisis-induced intermittency," Phys. Rev. A **36**, 5365–5380 (1987).

Grebogi, C., Ott, E., and Yorke, J. A., "Chaotic attractors in crisis," Phys. Rev. Lett. **48**, 1507–1510 (1982).

Grebogi, C., Ott, E., and Yorke, J. A., "Are three-frequency quasiperiodic orbits to be expected in typical nonlinear dynamical systems?" Phys. Rev. Lett. **51**, 339–342 (1983).

Halcrow, J., Gibson, J. F., Cvitanović, P., and Vismanath, D., "Heteroclinic connections in plane couette flow," J. Fluid Mech. **621**, 365–376 (2009).

He, K., "Riddling of the orbit in a high dimensional torus and intermittent energy bursts in a nonlinear wave system," Phys. Rev. Lett. **94**, 034101 (2005).

Heagy, J. F., Platt, N., and Hammel, S. M., "Characterization of on-off intermittency," Phys. Rev. E **49**, 1140–1150 (1994).

Hollerbach, R., "Non-axisymmetric instabilities in magnetic spherical Couette flow," Proc. R. Soc. A **465**, 2003–2013 (2009).

Hollerbach, R. and Skinner, S., "Instabilities of magnetically induced shear layers and jets," Proc. R. Soc. A **457**, 785–802 (2001).

Kantz, H. and Grassberger, P., "Repellers, semi-attractors, and long-lived chaotic transients," Physica D **17**, 75–86 (1985).

Kaplan, E. J., "Saturation of nonaxisymmetric instabilities of magnetized spherical Couette flow," Phys. Rev. E **89**, 1–8 (2014).

Kaplan, E. J., Nataf, H.-C., and Schaeffer, N., "Dynamic domains of the Derviche Tourneur sodium experiment: Simulations of a spherical magnetized Couette flow," Phys. Rev. Fluids **3**, 034608 (2018).

Kasprzyk, C., Kaplan, E., Seilmayer, M., and Stefani, F., "Transitions in a magnetized quasi-laminar spherical Couette flow," Magnetohydrodynamics **53**, 393–401 (2017).

Kawahara, G., Uhlmann, M., and van Veen, L., "The signficance of simple invariant solutions in turbulent flows," Arch. Ration. Mech. Anal. **44**, 203–225 (2012).

Knobloch, E. and Moehlis, J., "Bursting mechanisms for hydrodynamical systems," in *Pattern Formation in Continuous and Cou- pled Systems: A Survey Volume*, edited by M. Golubitsky, D. Luss, and S. Strogatz (Springer, New York, 1999) pp. 157–174.

Kuznetsov, A., Sataev, I., and Turukina, L., "On the road towards multidimensional tori," Commun. Nonlinear Sci. Numer. Simul. **16**, 2371 – 2376 (2011).

Lai, Y.-C., Życzkowski, K., and Grebogi, C., "Universal behavior in the parametric evolution of chaotic saddles," Phys. Rev. E **59**, 5261–5265 (1999).

Laskar, J., "Frequency analysis for multi-dimensional systems. Global dynamics and diffusion," Physica D **67**, 257–281 (1993a).

Laskar, J., "Frequency analysis of a dynamical system," Celestial Mech. Dyn. Astron. **56**, 191–196 (1993b).

Laskar, J., Froeschlé, C., and Celletti, A., "The measure of chaos by the numerical analysis of the fundamental frequencies. application to the standard mapping," Physica D **56**, 253 – 269 (1992).

Lemoult, G., Shi, L., Avila, K., Jalikop, S. V., Avila, M., and Hof, B., "Directed percolation phase transition to sustained turbulence in Couette flow," Nature Phys **12**, 254–258 (2016).

Letellier, C., "Intermittency as a transition to turbulence in pipes: A long tradition from reynolds to the 21st century," Comptes Rendus Mécanique **345**, 642–659 (2017), a century of fluid mechanics: 1870–1970.

Lilienkamp, T. and Parlitz, U., "Terminal transient phase of chaotic transients," Phys. Rev. Lett. **120**, 094101 (2018).

Lorenz, H.-W. and Nusse, H. E., "Chaotic attractors, chaotic saddles, and fractal basin boundaries: Goodwin's nonlinear accelerator model reconsidered," Chaos, Solitons & Fractals **13**, 957–965 (2002).

Matthaeus, W. H., Wan, M., Servidio, S., Greco, A., Osman, K. T., Oughton, S., and Dmitruk, P., "Intermittency, nonlinear dynamics and dissipation in the solar wind and astrophysical plasmas," Phil. Trans. R. Soc. Lond. A **373**, 20140154 (2015).

Moffatt, K. and Dormy, E., *Self-Exciting Fluid Dynamos*, Cambridge Texts in Applied Mathematics (Cambridge University press, 2019).

Morley, N. B., Burris, J., Cadwallader, L. C., and Nornberg, M. D., "GaInSn usage in the research laboratory," Review of Scientific Instruments **79**, 056107 (2008).

Newhouse, S., Ruelle, D., and Takens, F., "Occurrence of strange axiom A attractors near quasiperiodic flows on t^m, $m \geq 3$," Commun. Math. Phys. **64**, 35–40 (1978).

Nornberg, M. D., Spence, E. J., Kendrick, R. D., Jacobson, C. M., and Forest, C. B., "Intermittent magnetic field excitation by a turbulent flow of liquid sodium," Phys. Rev. Lett. **97**, 044503 (2006).

Ogbonna, J., Garcia, F., Gundrum, T., Seilmayer, M., and Stefani, F., "Experimental investigation of the return flow instability in magnetized spherical Couette flows," Phys. Fluids **32**, 124119 (2020).

Ogbonna, J., Garcia, F., Gundrum, T., Seilmayer, M., and Stefani, F., "Dynamic transitions of the magnetized spherical couette flow between its base state and the return flow instability," IOP Conf. Ser.: Mater. Sci. Eng. **1223**, 012004 (2022).

Oliveira, D. N., Rempel, E. L., Chertovskih, R., and Karak, B. B., "Chaotic transients and hysteresis in an α^2 dynamo model," J. Phys. Complex. **2**, 025012 (2021).

Omel'chenko, O. E. and Tél, T., "Focusing on transient chaos," J. Phys. Complex. **3**, 010201 (2022).

Ott, E. and Sommerer, J. C., "Blowout bifurcations: the occurrence of riddled basins and on-off intermittency," Phys. Lett. A **188**, 39–47 (1994).

Ott, E., Sommerer, J. C., Antonsen, T. M., and Venkataramani, S., "Blowout bifurcations: Symmetry breaking of spatially symmetric chaotic states," in *Lévy Flights and Related Topics in Physics*, edited by M. F. Shlesinger, G. M. Zaslavsky, and U. Frisch (Springer Berlin Heidelberg, Berlin, Heidelberg, 1995) pp. 182–195.

Philip, J. and Manneville, P., "From temporal to spatiotemporal dynamics in transitional plane Couette flow," Phys. Rev. E **83**, 036308 (2011).

Platt, N., Hammel, S. M., and Heagy, J. F., "Effects of additive noise on on-off intermittency," Phys. Rev. Lett. **72**, 3498–3501 (1994).

Platt, N., Spiegel, E. A., and Tresser, C., "On-off intermittency: A mechanism for bursting," Phys. Rev. Lett. **70**, 279–282 (1993).

Pomeau, Y. and Manneville, P., "Intermittent transition to turbulence in dissipative dynamical systems," Commun. Math. Phys. **74**, 189–197 (1980).

Pratt, J.,, Busse, A.,, and Müller, W.-C.,, "Fluctuation dynamo amplified by intermittent shear bursts in convectively driven magnetohydrodynamic turbulence," Astron. & Astrophys. **557**, A76 (2013).

Rand, D., "Dynamics and symmetry. Predictions for modulated waves in rotating fluids," Arch. Ration. Mech. Anal. **79**, 1–37 (1982).

Raynaud, R. and Dormy, E., "Intermittency in spherical Couette dynamos," Phys. Rev. E **87**, 033011 (2013).

Roberts, P. H. and Glatzmaier, G. A., "Geodynamo theory and simulations," Rev. Mod. Phys. **72**, 1081–1123 (2000).

Sánchez, J., Garcia, F., and Net, M., "Computation of azimuthal waves and their stability in thermal convection in rotating spherical shells with application to the study of a double-Hopf bifurcation," Phys. Rev. E **87**, 033014/ 1–11 (2013).

Sisan, D. R., Mujica, N., Tillotson, W. A., Huang, Y. M., Dorland, W., Hassam, A. B., Antonsen, T. M., and Lathrop, D. P., "Experimental observation and characterization of the magnetorotational instability," Phys. Rev. Lett. **93**, 114502 (2004).

Sommerer, J. C. and Ott, E., "A physical system with qualitatively uncertain dynamics," Nature **365**, 138–140 (1993).

Sweet, D., Ott, E., Antonsen, T. M., Lathrop, D. P., and Finn, J. M., "Blowout bifurcations and the onset of magnetic dynamo action," Phys. Plasmas **8**, 1944–1952 (2001).

Toniolo, C., Provenzale, A., and Spiegel, E. A., "Signature of on-off intermittency in measured signals," Phys. Rev. E **66**, 066209 (2002).

Travnikov, V., Eckert, K., and Odenbach, S., "Influence of an axial magnetic field on the stability of spherical Couette flows with different gap widths," Acta Mech. **219**, 255–268 (2011).

Tuckerman, L. S., "Computational challenges of nonlinear systems," in *Emerging Frontiers in Nonlinear Science*, edited by P. Kevrekidis, J. Cuevas-Maraver, and A. B. Saxena (Springer, New York, 2020) pp. 249–277.

van Veen, L. and Kawahara, G., "Homoclinic tangle on the edge of shear turbulence," Phys. Rev. Lett. **107**, 114501 (2011).

Venkataramani, S. C., Antonsen, T. M., Ott, E., and Sommerer, J. C., "Characterization of on-off intermittent time series," Phys. Lett. A **207**, 173–179 (1995).

Venkataramani, S. C., Antonsen, T. M., Ott, E., and Sommerer, J. C., "On-off intermittency: Power spectrum and fractal properties of time series," Physica D **96**, 66–99 (1996).

Yue, X., Xu, W., and Wang, L., "Global analysis of boundary and interior crises in an elastic impact oscillator," Commun. Nonlinear Sci. Numer. Simul. **18**, 3567–3574 (2013).